Transportation Research Part C 132 (2021) 103367

Contents lists available at ScienceDirect

Transportation Research Part C

journal homepage: www.elsevier.com/locate/trc

Modeling the effect of sensor failure on the location of counting sensors for origin-destination (OD) estimation

Mostafa Salari [a], Lina Kattan [a,*], William H.K. Lam [b], Mohammad Ansari Esfeh [a], Hao Fu [b]

[a] Department of Civil and Environmental Engineering, Schulich School of Engineering, University of Calgary, Calgary, Alberta, Canada
[b] Department of Civil and Environmental Engineering, The Hong Kong Polytechnic University, Hung Hom, Kowloon, Hong Kong, China

ARTICLE INFO

Keyword:
Network sensor location problem
Origin-Destination estimation
Sensor failure
Nonhomogeneous Poisson process
Genetic algorithm
OD demand information loss
OD demand reliability

ABSTRACT

The network sensor location problem (NSLP) for origin–destination (OD) estimation identifies the optimal locations for sensors to estimate the vehicular flow of OD pairs in a road network. Like other measurement apparatuses, these sensors are subject to failure, which can affect the reliability of the OD estimations. In this paper, we propose a novel model that allows us to solve the NSLP for OD demand estimation by identifying the most reliable locations to install sets of sensors with consideration for a nonhomogeneous Poisson process to account for time-dependent sensor failure. The proposed model does not rely on the assumption that true OD demand information is known. We introduce two separate objective functions to minimize the maximum possible information loss (MPIL) associated with OD demand on sensor-equipped links and OD pairs during the lifetimes of the sensors. Both objective functions are formulated to incorporate the possibility of sensor failure into the calculated OD demands. We use stochastic user equilibrium (SUE) to address the stochasticity of traffic route selection. We then employ the weighted sums method (WSM) and an ε-constraint to incorporate the objective functions into an integrated formulation. Two sensor types with different time-dependent failure rates are considered to identify the optimal locations for sets of sensors for OD demand estimation purposes while addressing the available budget constraints. We also address the problem of scheduled/routine maintenance of existing sensors by introducing an additional sensor deployment phase that focuses on maintaining the reliability of information by repairing or replacing failed sensors, installing additional sensors or a combination of both. The numerical results from the proposed model demonstrate how the deployment of more advanced sensors with lower failure rates can effectively improve the reliability of the information obtained from sensors. We also evaluate the use of different weights for the WSM's objective functions to explore alternative combinations of sensor configurations. The introduction of additional sensors to a network shows that the decision between repairing failed sensors and installing new sensors is highly dependent on the available budget and the failed sensors' locations.

* Corresponding author.
E-mail address: Lkattan@ucalgary.ca (L. Kattan).

https://doi.org/10.1016/j.trc.2021.103367
Received 25 January 2021; Received in revised form 23 August 2021; Accepted 25 August 2021
Available online 15 September 2021

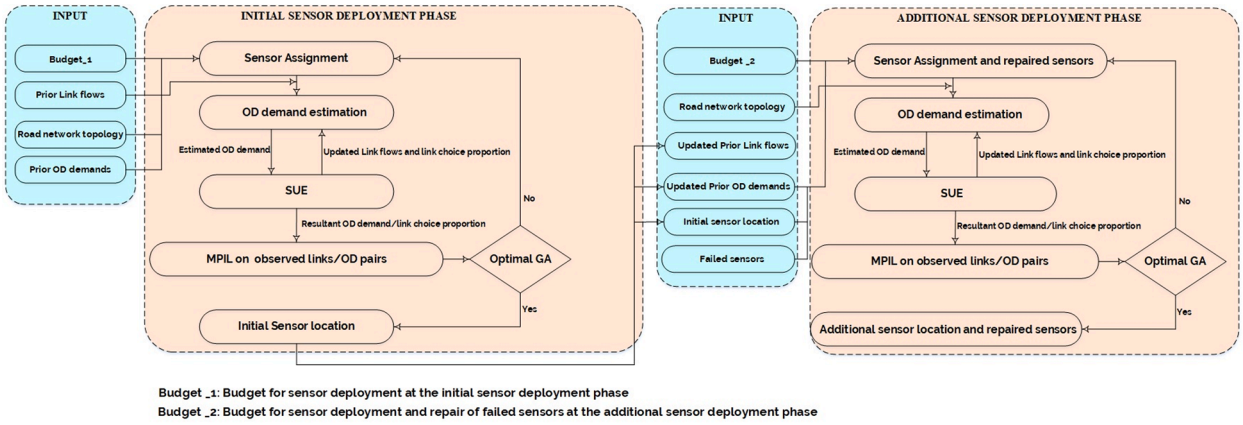

Fig. 1. Flowchart of the initial sensor deployment and additional sensor deployment phases.

1. Introduction

Origin-Destination (OD) demand reflects the OD pattern distribution of vehicular flows in a road network, which is typically divided into traffic analysis zones (TAZs). OD demand cannot be observed directly, so traffic surveys, which are labor-intensive and time-consuming, have traditionally been conducted to estimate demand between OD pairs or between TAZs. Technology advancements have allowed the development of new methods for traffic detection for OD demand estimation. One of these methods, based on traffic counting sensors, is frequently mentioned in the literature (Cascetta and Postorino, 2001).

While traffic count information is still viable in current traffic management applications, the counting sensors that provide this information are subject to considerable failure rates that adversely affect the quality and reliability of the information that sensors can deliver (Zhu et al., 2017; Salari et al., 2019). Danczyk et al., (2016) indicated that the explicit cost of repairing failed sensors might be too high for traffic management agencies' limited maintenance budgets. Sensor failure also imposes an implicit cost to these agencies due to the resulting loss of relevant and reliable traffic information. Since the information from these sensors can be inferred to estimate OD flows, the locations of the sensors can determine the availability and reliability of OD demand estimates between each OD pair in a road network. Placing sensors in strategic locations can also have a positive impact on the intensity of traffic flow that can be directly observed by sensors that are deployed on links. A robust sensor configuration can reduce the possibility of missing out on the necessary OD data for demand estimation and can prevent OD traffic flow information loss in the event of a sensor failure. Creating a sensor configuration that can minimize the effect of sensor failure on the OD estimation process is thus the main motivation behind this research.

In the literature on the network sensor location problem (NSLP), traffic flow information that is obtained from sensors deployed in a network is usually broken into two categories: traffic flow information from sensor-equipped links[1], (e.g., Salari et al., 2019, Viti et al., 2014) and traffic flow information from OD pairs (e.g., Cantelmo and Viti, 2020; Yang and Zhou, 1998)[2]. For instance, among the comprehensive set of rules for deploying sensors in a road network to estimate OD demand developed by Yang and Zhou (1998), OD covering rule concerns with the traffic flow information gain from OD pairs and the link independence rule addresses the traffic flow information from observed links. In accordance with previous studies, we also studied the traffic flow information associated with each OD pair and with each observed link, with consideration for the impact of sensor failure on the traffic flow information gain from both OD pairs and observed links.

Our research makes three primary contributions to the literature. First, we formulate a new mathematical model that considers the effect of sensor failure on the OD demand flow information loss in two categories: OD demand flow information loss for observed links and OD demand flow information loss for each OD pair. Since true OD demand information is not known in practice, the model identifies the optimal sensor locations by developing a metric to consider the maximum possible distance between the true and the estimated OD demands. In addition to identifying the maximum possible OD demand estimation error, our proposed metric also incorporates the possibility of sensor failure. We specifically address the (OD demand flow) Maximum Possible Information Loss (MPIL) that can occur due to both possible sensor failure and estimation errors for observed links and individual OD pairs. The second contribution considers the failure rates of sensors as a function of time by examining OD demand information loss during the sensors' wear-in, useful life, and wear-out phases. Consideration of sensors' time-dependent failure rates allows traffic authorities to monitor OD demand information loss through the deployed sensors' lifespans. The third contribution of this research divides the sensor deployment into two phases: an initial sensor deployment phase that considers the sensor location problem for a road network with no sensors deployed, and an additional sensor deployment phase, where the rules of initial sensor deployment are revised to install

[1] For the remainder of the paper, sensor-equipped links are called "observed links".
[2] Some other information, such as path flow information can be inferred from OD flow information

Table 1
Table of nomenclature.

Sets	
J	Set of OD pairs $J = \{1, ..., \|J\|\}$
L	Set of links $L = \{1, ..., \|L\|\}$
$\widetilde{L}$	Set of observed links at the initial sensor deployment phase $\widetilde{L} \subseteq L$
$\widetilde{L}'$	Set of observed links at the additional sensor deployment phase $\widetilde{L}' \subset L$
K	Set of sensor type $K = \{1, ..., \|K\|\}$
S	Set of sensor lifetime horizon
Subscripts	
j	Subscript of OD pairs
l	Subscript of links
k	Subscript of sensor type
s	Subscript of time horizon
Parameters	
q_j^{prior}	Prior OD demand information of OD pair j
$t_{l,j}$	Link choice proportion for link l and OD pair j
$\varphi_{l,j}$	Link-OD incidence matrix element for link l and OD pair j
$\left\{\widetilde{v}_l\right\}_{(n\times 1)}$	Column vector of observed traffic flow
$\lambda_k(s)$	Function of failure rate of sensor type k at time s
$f(s)$	Function of a nonhomogeneous Poisson process
$F_k(s)$	Probability of failure of sensor type k by time s
$R_k(s)$	Reliability of sensor type k at time s
$\vartheta_{l,s}$	Binary parameter that equals 1 if the sensor installed on link l at the initial sensor deployment phase still works at the time s. If the sensor installed on link l has failed by time s or if there is not a sensor deployed on that link, then $\vartheta_{l,s} = 0$.
w_1, w_2	Weights of the objective functions in WSM
c_k	Installation cost of sensor type k
$c_k^{'}$	Repair cost of sensor type k
η	Budget constraint at the initial sensor deployment phase
$\eta^{'}$	Budget constraint at the additional sensor deployment phase
ξ	Large positive constant
Variables	
$x_{k,l}$	Binary variable that determines if the sensor type k is installed on link l at the initial sensor deployment phase
$x_{k,l}^{'}$	Binary variable that determines if the sensor type k is installed on link l at the additional sensor deployment phase
$y_{k,l}^{'}$	Binary variable that determines if the sensor type k which is installed on link l at initial sensor deployment phase, is repaired due to the failure.
$\beta_{j,s}$	MPIL on OD j at time s
$\alpha_{l,s}$	MPIL on an observed link l at time s
ς_j	Relative difference between the estimated and true mean OD demand flows. It is a continuous variable that evaluates the accuracy of OD demand estimation for OD j, $\varsigma_j > -1$
$\partial_s^1 \& \partial_s^2$	Upper bounds for min–max objective functions
$\partial_s^{1'} \& \partial_s^{2'}$	Upper bounds for min-sum objective functions
q_j	Estimated mean OD demand of OD j at the initial sensor deployment phase
$q_j^{'}$	Estimated mean OD demand of OD j at the additional sensor deployment phase
Q_j	Multi-variate random variable for estimated OD demand of OD j
$E(v_l)$	Sample mean peak hour traffic flow on link l
v_l	Peak hour traffic flow on link l

additional sensors in the road network to minimize the OD demand information loss in the event of possible sensor failure. Deployment of additional sensors addresses the maintenance of existing sensors and allows the assumption that if an operating sensor fails, it can be either repaired or replaced.

Fig. 1 illustrates this study's framework, including the inputs and procedures for the initial sensor deployment and additional sensor deployment phases. The inputs for the initial sensor deployment phase include budget, the road network's topology, prior link flow, and prior OD demand. Given the absence of traffic sensors in this phase, some inputs, including prior link flow and OD demand,

Table 2
Categories of the estimation problem.

Estimation problem type	Examples of Studies
Estimation of OD flows using traffic count information	Chootinan et al., 2005; Doblas and Benitez, 2005; Ehlert et al., 2006; Fu et al., 2019; Gan et al., 2005; Kattan and Abdulhai, 2012; Yang et al., 1991; Yang and Zhou, 1998; Eisenman et al., 2006;
Estimation of link flow using traffic count information	Hu et al., 2009; Castillo et al., 2013
Estimation of link flow based on observations provided by image sensors	Bianco et al., 2006
Estimation of path flow using path ID sensors	Cerrone et al., 2015; Fu et al., 2016; Gentili and Mirchandani, 2005
Estimation of OD flow using vehicle ID sensors	Castillo et al., 2008; Hadavi and Shafahi, 2016,2019; Mínguez et al., 2010, Zhou and List, 2010;
Estimation of path flow based on the traffic information provided by vehicle ID sensors	Castillo et al., 2008; Mínguez et al., 2010

can be generated by a regional travel demand model (RTDM)[3] or collected using large-scale surveys such as household interviews, roadside interviews, license plate surveys, GPS traces, or cell phone data. While the additional sensor deployment phase has some inputs in common with the initial sensor deployment, the values and applications of the inputs between the two phases are not necessarily identical. For instance, both phases include a budget input. The budget for the initial sensor deployment phase determines the number and the type of sensors that can be initially installed in a road network, while the budget for the additional sensor deployment phase can be used to repair failed sensors, replace failed sensors, or install new sensors. In the additional sensor deployment phase, the previous link flow and OD demand values can be updated using the information collected from the sensors deployed in the initial phase in addition to the sources of prior OD information listed above. We therefore named these two inputs "Updated prior link flows" and "Updated prior OD demands" to reflect the use of traffic information from the initial sensors. Two inputs are unique to the additional sensor deployment phase: initial sensor location and failed sensors. These inputs contain the initial sensors locations determined by the initial sensor deployment phase and information about sensors that have failed when the additional sensor deployment phase is conducted.

Some procedures are implemented in both the initial and additional sensor deployment phases. In both phases, for example, the sensor assignment procedure leverages the observed link flow information to estimate OD demand. SUE is used to guarantee that the stochasticity of link-choice proportion is incorporated into the OD demand estimation process. After the OD demand values are estimated, it is possible to infer the OD demand information loss for observed links (i.e., sensor-instrumented links), and OD pairs. A Genetic Algorithm (GA) is used to present the possible sensor configuration of a road network and to find a local optimal solution that meets the GA's termination criteria. If the current sensor assignment meets the termination criteria, then that configuration is presented as the local optimal sensor location. Otherwise, the sensor assignment is updated and a similar procedure for OD demand estimation and OD demand flow information loss on observed links/OD pairs is repeated.

The remainder of this paper is organized as follows. We provide a brief literature review in Section 2. A simple example to demonstrate the motivation behind this study is described in Section 3. We then discuss the failure rate pattern and the effects of sensor failure on sensor location for the OD demand estimation process in Sections 4 and 5, respectively. We provide Table 1 to introduced all the notations employed throughout the paper. Section 6 presents the solution algorithm for solving the proposed model. The numerical results from applying the model on three example networks are reported and discussed in Section 7. Finally, we conclude the work with highlights and major findings of this research and recommend directions for future research in Section 8.

2. A literature review of sensor location for OD estimation purposes

The NSLP can be divided into two main branches: the flow observability problem and the flow estimation problem (Gentili and Mirchandani, 2012). Models that address the flow observability problem identify the best locations that will allow sensors to uniquely determine the target flow. Models that address the flow estimation problem define certain conditions for the locations of sensors in a road network that will allow them to obtain the best estimate of the target flows. For both problems, identifying the locations and the number of sensors necessary to determine the target flow is a seminal step (Bianco et al., 2001; Hu et al., 2009; Rubin and Gentili, 2021).

Using the four different types of sensors defined by Gentili and Mirchandani (2012) (i.e., counting, path-ID, image, and vehicle-ID) and the target estimated flows (i.e., link, route, and/or OD flows), twelve distinct categories can be considered for the sensor location aspect of the OD estimation problem (Hadavi and Shafahi, 2016). Table 2 illustrates examples of popular categories and the key literature related to each of them. You may note that some categories have received more attention in the literature than others.

Other studies have investigated the use of a combination of sensors (e.g., vehicle ID sensors and counting sensors) to identify optimal sensor locations and to estimate target flows (e.g., Zhou and List, 2010). Readers can refer to Viti et al. (2014) and Hadavi and Shafahi (2016) for a more extensive literature review on identifying the locations of traffic sensors for estimation purposes.

This research uses traffic counts as a source of information for reliable OD estimation, so a thorough review of studies that focus on using traffic count information to address the reliability of estimation in the sensor location OD estimation problem is required. The

[3] Readers can refer to the following website for more information about the RTDM: https://www.rtc.wa.gov/data/model/demand/. They can also refer to the following references: de Dios Ortúzar and Willumsen, 2011; Florian; 2008; Meyer and Miller, 1984).

related work of Gan et al., (2005) recommended using the possible relative error (PRE), which evaluates the expected value of the relative OD estimation error, instead of the maximum possible relative error (MPRE) initially developed by Yang et al., (1991), which measures the quality of the OD estimation. The MPRE measures the maximum possible deviation between the estimated OD vector and any OD vector in the feasible OD space, while the PRE represents the expected distance between the estimated OD vector and a random feasible OD vector. Yang et al., (2006) proposed a mixed-integer programming formulation to determine the number of OD pairs whose flows can be specified for a given number of sensors. Their proposed formulation determined the minimum number of sensors required to capture the demands of all OD pairs. In a similar, more recent study, Owais et al., (2019) presented a robust sensor location model that determines the ideal number of sensors and their optimal locations while attempting to reduce the MPRE boundary for an estimated OD matrix.

Other studies have proposed other metrics to evaluate the quality of OD estimates. For instance, Bierlaire (2002) recommended the use of a total demand scale (TDS) to measure the quality of an OD estimation. Ehlert et al., (2006) developed a linear integer model to identify the ideal locations of counting sensors. Their proposed formula introduces an index of importance for each OD pair and then maximizes the sum of these indices for the covered pairs in the objective function. Ehlert et al., (2006) declared that the linear programming (LP) sub-problem provides an upper bound and can be easily employed for medium- and large-sized networks. Chootinan et al. (2005) formulated a bi-objective traffic counting location problem for OD trip estimation. Their proposed model simultaneously employs two contradictory criteria, minimal resource utilization, and maximum coverage, to strike a balance between the estimation quality and the coverage cost.

2.1. OD demand estimation methods and prior OD information

OD demand estimation methods can be classified based on the network configuration and the time horizon (Chen et al., 2004). Proposed models in the literature that address network configuration tend to consider simple networks with no route choice effect, networks with no congestion (i.e., proportional assignment) (e.g., Hazelton, 2003; Lo et al., 1999), and networks with both route choice and congestion (e.g., Lu et al., 2015; Nigro et al., 2018; Qurashi et al., 2020; Zhang et al., 2021). Concerning the time horizon, the models are either time-independent (also known as static) (e.g., Bell, 1991; Hazelton 2000) or time-dependent (also known as dynamic) (e.g., Balakrishna et al., 2019; Cao et al., 2021; Osorio, 2019). OD demand models were first developed in the static context where "average" peak hour OD demands are estimated by leveraging average peak hour traffic counts collected across a relatively long time period. The drawback of static models is that the time-varying nature of OD demand is not considered. The OD demand estimation model used in this work falls within the static category, which considers the congestion and route choice in a road network. With additional work, however, the proposed model can be expanded to incorporate time-dependent OD demand estimation with consideration for time-dependent traffic counts. We limited this work to static OD demand to focus on the work's primary contribution, which is the *effect* of sensor failure on OD demand estimation. Combining time-dependent OD demand estimation models with the time-dependent failure rates of sensors could be an interesting future research direction.

In this work, it is assumed that other type of information such as the GPS and cellular data can be used to obtain the prior OD demand that is used as *inputs* for the OD demand estimation in both the initial and additional sensor deployment phases. Since we focused on the sensor location problem, we limited our consideration for traffic data extracted from the sensors installed on links for the purpose of OD demand estimation. Along with traffic counts, however, GPS traces and cellular data can be embedded into the OD demand estimation process for more robust data[4]. These new sources of information can reduce or eliminate OD demand information loss due to sensor failure as the information provided by GPS and phone data can compensate for the missing data from the failed sensor. Another reason for avoiding these newer sources of information in our initial research is that they often suffer from a low penetration rate. To add these new data sources for future research, the OD demand information loss for an OD pair can be redefined as a situation when the sensors traversed by that OD pair fail and the penetration rate of GPS traces and cellular data for that OD pair is less than a certain value. Revising the proposed MPIL and OD demand estimation processes to incorporate more advanced sources of information is another interesting potential research path.

2.2. The importance of MPIL in the state of art

In the OD demand estimation literature, statistical measures are used to quantify the quality of OD demand estimates. Examples of the statistical measures include, but are not limited to, mean absolute error (MAE), root mean square error (RMSE), and total demand deviation (TDD)[5]. These measures evaluate the closeness between true and estimated OD demands. Since true OD demands are rarely known in practice, these statistical measures are not practical methods of quantifying the quality of OD demand estimation. Other measures like MPRE (Yang et al., 1991), PRE (Gan et al., 2005), and TDS (Bierlaire, 2002) focus on estimating the error bound of the OD demand estimation. With respect for the quality of OD demand estimation and in line with MPRE, MPIL addresses the worst possible error bounds by estimating the error bounds under the assumption that the true OD demand values are not available. MPIL offers quality estimates, while also addressing the possibility of losing a certain level of quality of OD demand estimation due to sensor failure. For instance, if all sensors that observe the flow of an OD pair fail, then the flow of that OD pair can no longer be estimated. In

[4] Readers can refer to Bachir et al., (2019) and Ge and Fukuda (2016) for more information on how the GPS traces and phone data can be embedded into the OD demand estimation model.

[5] Readers can refer to Chen et al., (2012) to find the detailed information of these measures.

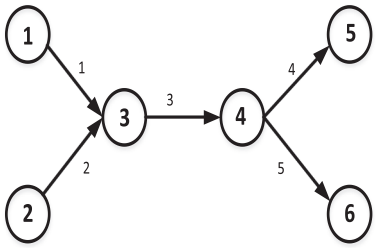

Fig. 2. Toy network.

Table 3
OD information related to different sensor location sets on the toy network presented in Fig. 2.

OD	Link flows[1] (1)v_l	Route	Estimated OD demand for sensor location set on the link[2]		Maximum deviation between the estimated and true OD demands[3]	
			1st set:$\{1,2\}$	2nd set: $\{3,4\}$	1st set:$\{1,2\}$	2nd set: $\{3,4\}$
1–5	$v_1 = 14$	{1,3,4}	7	7.5	1	1
1–6	$v_2 = 7$	{1,3,5}	7	3	−1	1
2–5	$v_3 = 21$	{2,3,4}	3.5	7.5	1	−1
2–6	$v_4 = 15$	{2,3,5}	3.5	3	1	−1
	$v_5 = 6$		MPRE[4]		1	1

v_l: the link flow of link l.
[1] The unit for OD demand is **(veh/hr)**.
[2] These estimated values are presented for the sake of this example. No specific method is employed to exploit these values.
[3] According to Yang et al. (1991), the relative deviation between the estimated OD demands and the true demands is greater than or equal to negative 1.
[4] The detailed calculation to compute MPRE for these location sets is explained in Appendix A.

this case, the error bounds of OD estimation for that OD pair will be equal to infinity.

Another important aspect associated with the statistical measures for OD demand estimation is the assumption of the independent distribution of OD demand in a road network. MPIL, like the previously discussed OD demand estimation measures, assumes that OD demand is independently distributed. There are, however, some recent studies that consider the correlation between OD pairs (e.g., Cantelmo et al., 2018; Cascetta et al., 2013; Fu et al., 2019). For instance, the weighted maximum possible relative error of covariance (WMPREC) developed by Fu et al., (2019) recognizes the potential dependency between OD pairs. Future extensions of this research should relax this assumption to incorporate the existing dependency between some OD pairs.

3. Example of the motivation behind this research

A small example will help to demonstrate the motivation behind this research. The toy network illustrated in Fig. 2 has two origins, nodes 1 and 2, and two destinations, nodes 5 and 6. Each origin point can end at one of the possible destinations. Fig. 2 depicts the flow and routes between each OD pair.

Table 3 shows the four OD pairings, the link flow information, the estimated OD information[6], and the links traversed by each OD flow in Fig. 2, respectively. Table 3 also shows two possible sensor location sets and possible OD estimates for each location set. Links 1 and 2 are instrumented with sensors in the first sensor location set, while links 3 and 4 are equipped with sensors in the second location set. For every observed link in each location set, the sum of the estimated OD demands that traverse that link should be equal to the link flow, assuming that there is no measurement error in the sensors' observations. For example, link 1 in the first sensor location set is instrumented with a sensor. The sum of the estimated OD demand of ODs 1–5[7] and 1–6, which traverse link 1, should be equal to the link flow of this link, which is $7 + 7 = 14$. Based on this explanation, the column of Table 3 entitled "Estimated OD demand for sensor location set on the link" show the estimated OD demand for each OD pair based on whether the sensor location set follows either the first or the second location set. In this example, we use the MPRE method to calculate the *maximum* possible deviation of estimated OD demands from their true values. The last column of Table 3 shows the maximum deviation between the estimated and true OD demands, which can be obtained through the calculation of MPRE (see Appendix A). The first and second sets of sensors have equal total maximum deviations of the MPRE from the true OD demands (see the final row in Table 3).

In this work, we explore how sensor failure can further contribute to the maximum deviation between the estimated OD demands and the true ones. We borrowed the values of maximum deviation between the estimated OD demands and the true ones from the last

[6] True OD information refers to information that can be used to evaluate the quality of OD estimates.
[7] OD 1–5 represents OD pair that originates from node 1 and terminates at node 5.

Table 4
Comparison of the relative deviation between the OD demands of the first and second sensor location sets with consideration of sensor failure.

OD	Expected value of maximum deviation between the estimated and true OD demands considering sensor failure (Assumption: sensors are identical)	
	1st set:$\{1,2\}$	2nd set:$\{3,4\}$
1–5	$\left(\frac{1}{1-p}\right)$	$\left(\frac{1}{1-p^2}\right)$
1–6	$\left(\frac{1}{1-p}\right)$	$\left(\frac{1}{1-p}\right)$
2–5	$\left(\frac{1}{1-p}\right)$	$\left(\frac{1}{1-p^2}\right)$
2–6	$\left(\frac{1}{1-p}\right)$	$\left(\frac{1}{1-p}\right)$

column of Table 3 and squared those values to cancel the effect of negative values. The squared values ranged from zero to infinity, where larger values imply a higher relative deviation between the estimated and true OD demands. If we divide the squared values of deviation between the estimated and the true OD demands by the probability of *not missing* the OD demand flow information, the results indicate how that sensor failure further contributes to the possible maximum deviation between the estimation of OD demand and the true OD value for each OD pair.

The term "*missing OD demand flow information*" refers to a situation where it is no longer possible to estimate the vehicular traffic demand of a given OD pair due to sensor failure. For an arbitrary OD pair, this situation occurs when all the sensors observing the flow of the OD pair break down (the OD covering rule by Yang and Zhou (1998)). We can use the first sensor location set, where the sensors are installed on links 1 and 2, as an example. The probability of this location set of sensors missing OD demand flow information from OD 1–5 will be p, where p is the probability of failure of the sensor installed on link 1. The probability of not missing the OD demand flow information of this OD pair is $1-p$. We can evaluate the expected value of the contribution of sensor failure into the maximum deviation of the estimated and true OD demand of OD 1–5 by dividing the squared relative deviation between the estimated OD demand and the true value of OD 1–5 by $1-p$. For instance, if $p=0$, then the maximum deviation between the estimated and true OD demand of OD 1–5 is only due to estimation error. Therefore, the lower the probability of missing the OD pair's OD demand flow information, the lower the expected value of the maximum deviation between the OD pair's estimated and true OD demand values.

Table 4 compares the two sensor location sets introduced in Table 3 with consideration for the impact of a possible sensor failure on the maximum deviation between each OD pair's estimated and true OD demand. For simplicity, all sensors are assumed to be identical in this example, with similar probabilities of failure. When we compare location sets, we favor the second location set over the first because it results in a lower total expected value of the maximum deviation between the estimated and true OD demand in the event of sensor failure. Simply put, for any value of p, $p<1$, the sum of the squared maximum deviation between the estimated and true OD demand divided by the probability of not missing the OD demand flow information for all OD demands in the second set is less than the same value for the first sensor location set: $\left(\frac{4}{1-p}\right) \geqslant \left(\frac{2}{1-p}\right)+\left(\frac{2}{1-p^2}\right)$.

Table 4 contains information about the probability of missing the OD demand flow for individual OD pairs, which can be used for traffic monitoring applications where some OD demands are of more interest to traffic management authorities than others. In the real world, the failure rates of sensors are not necessarily identical or constant over time, and the flow between each OD pair exhibits random rather than deterministic behavior. This simple example also does not consider alternative routes since each OD had only one route choice. The problem becomes more complicated once route choice must be determined as part of the OD estimation problem. To address the above-mentioned viewpoints, we propose a new formulation that identifies the most reliable non-identical sensor locations in a road network to minimize the impact of sensor failure on the OD estimation process.

4. Failure rates and the mean lifetimes of traffic sensors

Reliability engineering and survival analysis of traffic sensors as a system focus primarily on the system's lifetime functionality, which is typically represented as one or more positive random variables. By using a random variable to represent the sensor system's lifetime, we can thoroughly characterize the sensor system through its distribution function. The culmination of a sensor system's lifetime is shown by its death, which is represented as a terminating event known as the failure incident. Knowledge of an operating system's failure behavior or pattern, especially the failure behaviors of sensors in a sufficiently small-time interval, is key to survival analysis of the system. Identifying the failure rate, or the frequency with which a system or a component of the system fails expressed per unit of time is the core component of determining a system's failure behavior. The failure rate of a sensor system or component typically varies over its life cycle. For example, the failure rate of a sensor in its tenth year of service might be greater than the failure rate of the same type of sensor in its first year of service.

4.1. Failure rates of sensors using nonhomogeneous Poisson process

The rate λ, also known as failure rate, in a Poisson process, $f(s)$, is the proportionality constant in the probability of an event happening during an arbitrary small time interval Δs:

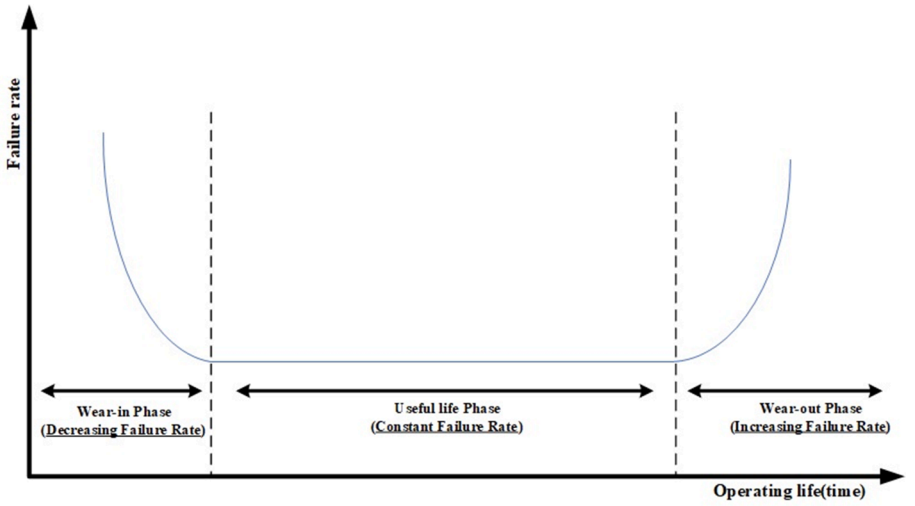

Fig. 3. Bathtub curve (Aarset, 1987).

$$Pr\{f(s+\Delta s)-f(s)=1\}=\frac{(\lambda\Delta s)e^{-\lambda\Delta s}}{1!}=(\lambda\Delta s)\left(1-\lambda\Delta s+\frac{1}{2}\lambda^2\Delta s^2-\ldots\right)=\lambda\Delta s+e(\Delta s) \tag{1}$$

where in Eq. (1), s is the time index and $Pr\{f(s+\Delta s)-f(s)=1\}$ shows the probability of one incident between time s and time $s+\Delta s$. Moreover, $e(\Delta s)$ denotes a general and unspecified remainder term of smaller than Δs. It is pertinent in different applications to assume that the rate is a Poisson process that varies with time, i.e., $\lambda=\lambda(s)$. Such a process is called the nonhomogeneous or nonstationary Poisson process to be distinguished from the stationary process with the constant failure rate (Kingman, 2005). If $f(s)$ is a nonhomogeneous Poisson process with a time-dependent rate, $\lambda(s)$, then an increment $f(s'+\Delta s)-f(s')$, giving the number of events in the range $(s', s'+\Delta s]$ has also a Poisson distribution with the parameter $\lambda'=\int_{s'}^{s'+\Delta s}\lambda(s)ds$. Considering nonhomogeneous Poisson process with the time-dependent failure rate, λ', the reliability of a system at time s' can be shown as $R(s')$:

$$\begin{aligned} R(s') &= Pr\{f(s')-f(0)=0\}=\frac{\lambda' e^{-\lambda'}}{0!}=\lambda' e^{-\lambda'} \\ \lambda' &= \int_0^{s'}\lambda(s)ds \end{aligned} \tag{2}$$

where $Pr\{f(s')-f(0)=0\}$ denotes the probability of no failure event occurring, between time zero and time s'. Accordingly, the reliability of a system at time s' shows the probability of no failure between the time interval $(0, s']$. The failure rate profile of a nonhomogeneous Poisson process is usually represented by the Bathtub curve. The bathtub curve, as shown in Fig. 3, can be segmented into three distinct time phases: wear-in, useful life, and wear-out. The wear-in phase is also known as the infant mortality phase. It is usually short, with a decreasing failure rate over time. The useful life, or youth, phase typically spans a longer period than the other two phases. If a device like a traffic sensor survives the wear-in phase, it exhibits a constant failure rate throughout its useful life phase. The wear-out, or aging phase, is the final phase of a product's lifecycle. During this phase, occurrences like material fatigue, corrosion, embrittlement, etc., result in device failure. When a sensor device enters this phase, it needs more frequent inspection, special maintenance, and, if required, complete replacement.

In the following section, we elaborate on how sensor failure can be incorporated into the sensor location for the OD demand estimation process.

5. The effect of sensor failure on sensor location for OD demand estimation

In this section, we investigate the significance of sensor failure on the MPIL for a road network. We begin by distinguishing between the impact that each sensor's failure would have on the MPIL for observed links and the impact of sensor failure on the MPIL for each OD pair. We then discuss these considerations with the assumption that the sensors are not necessarily identical and might therefore exhibit dissimilar failure behaviors. We considered two phases of sensor deployment: initial sensor deployment and additional sensor deployment. These phases are assumed to occur in chronological order, where the initial sensor deployment occurs before the additional sensor deployment. The initial sensor deployment corresponds with long-term planning for a road network and takes place the first time sensors are ever deployed on the road network. Additional sensor deployment is associated with road networks that already have sensors deployed and is a recurring phase that occurs during scheduled or routine maintenance. Depending on whether

the current status of existing sensors is failed or functional, either failed sensors will be repaired or replaced, or additional sensors will be added to the road network.

We assume in this study that sensors are deployed independently, so there is no spatial or temporal correlation between the failure of any pair of sensors. We also assume that a road network consists of $|J|$ OD pairs and $|L|$ links, where $J$and L denote the set of OD pairs and links within the network, respectively. Let the binary variable $x_{k,l}$ indicate whether a link l is instrumented with sensor type k ($k \in K$) at the initial sensor deployment phase, where $\sum_{k\in K} x_{k,l} = 1$ denotes that this link is equipped with a sensor and is therefore referred to as an observed link, and 0 means the link is not equipped with a sensor. To represent all traffic sensor locations in the road network, we define set $\widetilde{L}$ as a subset of L, where $\widetilde{L} = \{l \in L | \sum_{k\in K} x_{k,l} = 1\}$. Set $\widetilde{L}$ is a function concerning the binary variable $x_{k,l}$: $\widetilde{L} = L(X)$, where $X = \left(.., \sum_{k\in K} x_{k,l}, ...\right)^T$. The random variable v_l represents the stochastic vehicular traffic flow observed on the observed link l, and $\left\{\widetilde{v}_l\right\}_{(n\times 1)}$ is a column vector that denotes the observed traffic flow, which can vary from weekday to weekday on the same link for the same observed period. The number of rows in the column vector n represents the number of measurements on link l where $\widetilde{v}_l^{(i)}$ is the i^{th} element of this vector, denoting the i^{th} measurement of traffic flow during the weekday peak hour period on link l.

We can use the following equation to calculate the sample mean peak hour traffic flow on link l with the information obtained from the column vectors of the observed traffic flows:

$$E(v_l) = \frac{1}{n}\sum_{i=1}^{n} \widetilde{v}_l^{(i)} \quad \forall l \in \widetilde{L} \tag{3}$$

If we represent the OD demand estimate for OD pair j during the same weekday peak hour period (Q_j) as a multivariate random variable in which $E(Q_j) = q_j$ where q_j is the estimated mean OD demand, then Eq. (4) is an alternative way of calculating v_l:

$$v_l = \sum_{j\in J} t_{l,j} Q_j \ \forall l \in \widetilde{L} \tag{4}$$

where $t_{l,j}$is the proportion of weekday peak hour traffic flow from OD j that uses link l. Since v_l and Q_j can vary from day to day, we accordingly assume in this research that $t_{l,j}$ is *not* a deterministic parameter for each link and OD demand, and that it must therefore be endogenously determined[8]. The sample mean of peak hour traffic flow associated with link l ($E(v_l)$) can thus be newly represented using Eq. (5):

$$E(v_l) = E\left(\sum_{j\in J} t_{l,j} Q_j\right) = \sum_{j\in J} t_{l,j} q_j \ \forall l \in \widetilde{L} \tag{5}$$

Eqs. (4) and (5) are both expressed for observed links. The sample mean of traffic flows obtained via link traffic counts provides vital information about the traffic flow pattern traversing each link. The following section explains the MPIL for OD pairs and observed links in more detail.

5.1. MPIL for each OD pair

Ideally, if the true OD is known for a road network, that information can be used to evaluate the quality of the estimated values for each OD demand. The ideal information gain for each OD pair occurs when the estimated mean OD demand equals the true mean OD demand. Any absolute deviation between these two values is an estimation error that can further contribute to the information loss for that OD pair. However, true OD demand information is not typically available to measure the true information gain for each OD pair. Therefore, in the proposed MPIL metric, we evaluate the maximum possible error in OD demand estimation expressed as maximum distance between the true and estimated mean OD demand on each OD. In addition to the error in the estimated OD demand, the failure probability of the sensors installed on links traversed by an OD pair can also affect the MPIL; thus, the higher the probability of sensor failure, the higher the information loss for that OD pair. The MPIL proposed below for OD pair j incorporates both the OD estimation error and the loss of information from the possible failure of sensors installed on links traversed by this OD pair:

$$\beta_j(s) = max\left(\left(1 - \prod_{k\in K} F_k(s)^{\left(\sum_{l\in L} \widetilde{\varphi_{l,j}} x_{k,l}\right)}\right)^{-1} \varsigma_j^2\right) \ \forall j \in J, s \in S \tag{6}$$

where $F_k(s)$ is the probability that the sensor type k fails by time s, i.e., $1 - R_k(s)$. Equation $\sum_{l\in M} \widetilde{\varphi_{l,j}} x_{k,l}$, which is the power of $F_k(s)$, calculates the number of observed links that are equipped with sensor type k and are traversed by OD pair j, where $\varphi_{l,j}$ is the element of the link-OD incidence matrix that signifies whether OD j traverses link l ($\varphi_{l,j} = 1$) or not ($\varphi_{l,j} = 0$). Moreover, ς_j equals $\left(\frac{q_j^* - q_j}{q_j}\right)$ where q_j^* is the true mean OD demand (q_j^*) for OD pair j as defined by Yang et al. (1991). The ideal situation in terms of minimizing OD demand

[8] In the following sections, we discuss the calculation procedure of the link choice proportion using SUE.

Table 5
The OD demand information gains for the OD pairs in Fig. 2.

OD	True mean OD demand	Estimated mean OD demand		ς_j^2		MPIL for OD demand $\beta_j(s')$	
		1st set:$\{1,2\}$	2nd set:$\{3,4\}$	1st set:$\{1,2\}$	2nd set:$\{3,4\}$	1st set:$\{1,2\}$	2nd set:$\{3,4\}$
1–5	10	7	*7.5*	0.18	0.11	$0.18\left(\frac{1}{e^{-\lambda' }}\right)$	$0.11\left(\frac{1}{1-(1-e^{-\lambda' })^2}\right)$
1–6	4	*3.5*	*3*	0.02	0.11	$0.02\left(\frac{1}{e^{-\lambda' }}\right)$	$0.11\left(\frac{1}{e^{-\lambda' }}\right)$
2–5	5	7	*7.5*	0.08	0.11	$0.08\left(\frac{1}{e^{-\lambda' }}\right)$	$0.11\left(\frac{1}{1-(1-e^{-\lambda' })^2}\right)$
2–6	2	*3.5*	*3*	0.18	0.11	$0.18\left(\frac{1}{e^{-\lambda' }}\right)$	$0.11\left(\frac{1}{e^{-\lambda' }}\right)$

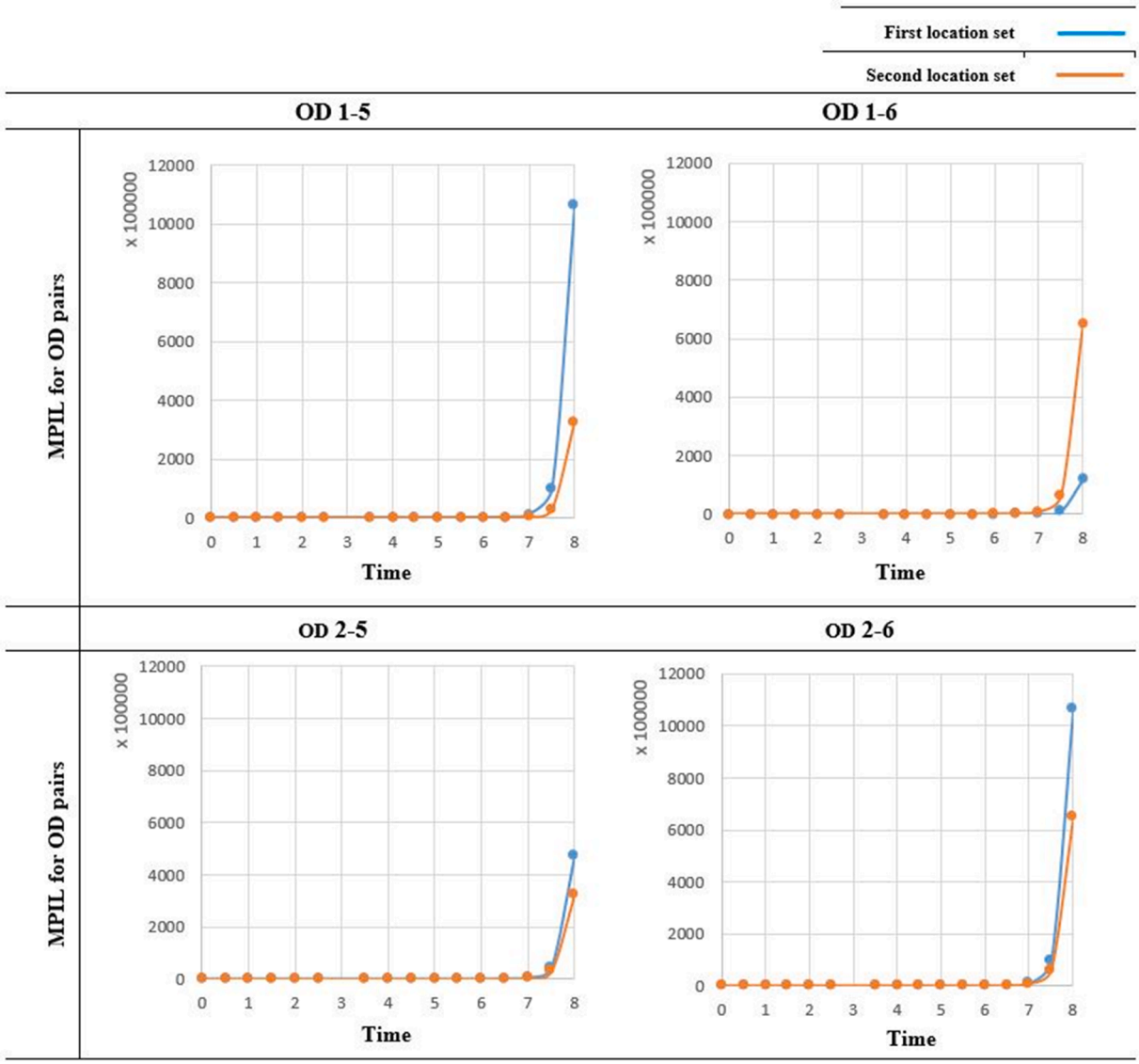

Fig. 4. MPIL graph of OD pairs for the first and the second sensor location sets.

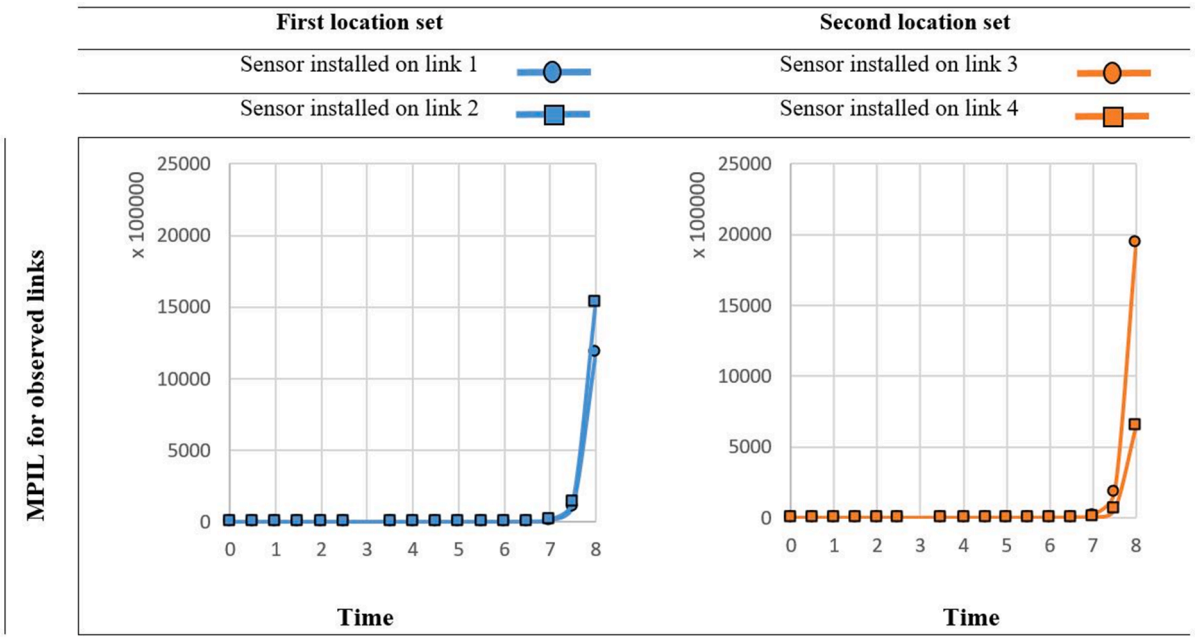

Fig. 5. MPIL graph of observed links for the first and the second sensor location sets.

information loss due to the sensor failure at time s is when the probability of missing the information necessary to estimate OD demand j is approximately zero ($\prod_{k\in K}F_k(s)^{\left(\sum_{l\in L}\sim\varphi_{lj}x_{kl}\right)} \approx 0$). In such a situation, $\left(1-\prod_{k\in K}F_k(s)^{\left(\sum_{l\in L}\sim\varphi_{lj}x_{kl}\right)}\right)^{-1}$ will be equal to 1 and any OD demand information loss will only occur due to the estimation error. On the other hand, the worst-case scenario in terms of OD demand information loss due to the failure of sensors at time s is when all the sensors installed on links that observed the OD demand j fail by time s, $\prod_{k\in K}F_k(s)^{\left(\sum_{l\in L}\sim\varphi_{lj}x_{kl}\right)} = 1$. In such a situation, $\left(1-\prod_{k\in K}F_k(s)^{\left(\sum_{l\in L}\sim\varphi_{lj}x_{kl}\right)}\right)^{-1}$ will be equal to zero and therefore $\beta_j(s)$ will be infinity. This definition is in line with the "OD covering" rule developed by Yang et al. (1991). According to the OD covering rule, if no sensor observes the OD demand j then the MPRE will be infinity. In Eq. (6), $\varsigma_j^2 = \left(\frac{q_j^*-q_j}{q_j}\right)^2$ represents the squared relative difference between the estimated and true mean OD demand flows, and thus reflects the information loss of the truemean OD demand for each OD pair. ς_j^2 is always greater than or equal to 0, where $q_j^*, q_j > 0$ ($\varsigma_j \geqslant -1 \rightarrow \varsigma_j^2 \geqslant 0$).

Let us build upon our toy network from Section 3 to elaborate more on maximum OD demand flow information loss for OD pairs. Assume that the "true" OD is known, and that two different estimated OD demands for each OD pair are inferred based on the two location sets of sensors introduced in Table 3. Moreover, let's assume the time-dependent failure rates of sensors are identical and are shown using the following piecewise function:

$$\lambda(s) = \begin{cases} 4-s & 0\leqslant s<2 \\ 2 & 2\leqslant s<5 \\ s-3 & s\geqslant 5 \end{cases} \tag{7}$$

$F(s')$for each sensor then can be calculated using the Poisson distribution, i.e., $F(s) = 1-\frac{(\lambda')^0 e^{-\lambda'}}{0!} = 1-e^{-\lambda'}$ where $\lambda' = \int_0^{s'}\lambda(s)ds$.

We can compare the MPIL for each OD pair in the first and the second location sets presented in Table 5. To do this, we set up a two-dimensional coordinate system where the horizontal axis represents the time s and the vertical axis shows the MPIL (Fig. 4). In each segment of Fig. 4, the blue and orange-highlighted curves belong to the MPIL for each OD pair of the first and the second location sets, respectively.

According to Fig. 4, the first location set of sensors has a higher MPIL for OD pairs 1–5, 2–5 and 2–6, where $0\leqslant s<8$. For OD pair 1–6, however, the second location set has a higher MPIL for the same range of s. It is interesting to observe OD 2–5, whose ς_j^2 is higher in the second location set than in the first location set, has lower MPIL in the second location set than that of the first location set, as more sensors are available to observe the flow of OD 2–5 in the second location set.

5.2. MPIL on an observed link

In addition to considering the impact of sensor failure on the demand information loss for each OD pair in a road network, we are

also interested in the effect of sensor failure on the OD demand information loss while traversing an observed link. In other words, we investigate the effect that the failure of each sensor would separately have on the aggregated OD demand flow information loss. The MPIL for an observed link focuses on the maximum possible OD demand loss on a sensor-equipped link. This maximum loss is associated with simultaneous sensor failure and estimation error. To obtain the maximum OD demand loss on observed link l at time s, we propose Eq. (8) which incorporates both the OD estimation error and the possibility that the sensors installed on this link fail:

$$\alpha_l(s) = max\left(\sum_{j\in J}\left(1-\left(\sum_{k\in K}(F_k(s))x_{k,l}\right)\right)^{-1} t_{l,j}\varsigma_j^2\right)\ \forall l\in\widetilde{L}, s\in S \tag{8}$$

where in Eq. (8), similar to Eq. (6), $F_k(s)$ is the probability of failure of sensor type k by time s and the link choice proportion $t_{l,j}$ is determined through SUE. According to Eq. (8), the OD demand flow information traversing link l cannot be estimated if the sensor installed on this link breaks down. Although subset $\widetilde{L}$ only considers links equipped with sensors, we must still include a binary variable $x_{k,l}$ to account for the type of sensor that is installed on the link l. In Eq. (8), the closer the value of the term $\left(1-\left(\sum_{k\in K}(F_k(s))x_{k,l}\right)\right)^{-1}$ to 1, the more the OD demand information loss is attributed to the estimation error. In other words, the ideal condition in terms of minimizing OD demand information loss due to the failure of a sensor is when the probability that the sensor installed on link l will fail is zero, $(F_k(s)=0)\Rightarrow\left(1-\left(\sum_{k\in K}(F_k(s))x_{k,l}\right)\right)^{-1}=1$ and therefore, the maximum OD information loss becomes merely associated with the OD estimation error $\alpha_l(s)=\sum_{j\in J} t_{l,j}\varsigma_j^2\ ,\forall l\in\widetilde{L}, s\in S$.

Fig. 5 shows the MPIL for the first and the second sensor locations in the toy network introduced in Table 3. The sensors in this figure are assumed to be identical and to follow the time-dependent failure rate introduced in Eq. (7). Similar to Fig. 4, Fig. 5 consists of a two-dimensional coordinate system where the horizontal axis shows the time s and the vertical axis represents the MPIL for observed links. As we assume the observation from sensors are free of error, the consideration of sensor failure cannot affect the estimation error, but a sensor with lower failure rate can improve MPIL. For instance, in the first sensor location set, observed link 1 has a lower MPIL than observed link 2 in the same location set where $0\leqslant s<8$. This means that if one of these sensors can be replaced with a sensor that has lower failure rate, then link 2 should be selected to improve MPIL on this link.

We can also observe that link 3 has the highest MPIL between the two location sets compared to the other sensors, as it also has the highest aggregated ς_j^2 among all other sensors. So, while the installation of more advanced sensor on this link cannot help with estimation error it can help decrease the MPIL to a level that failure rate of sensor has minimum effect on the MPIL of this observed link.

5.3. Properties of $\beta_j(s)$ and $\alpha_l(s)$

The MPIL on observed links, $\alpha_l(s)$, and for each OD demand, $\beta_j(s)$, have upper bounds provided that the maximum covering rule introduced by Yang et al. (1991) is satisfied. With the OD covering rule, we can define the following equation:

$$\sum_{j\in J}t_{l,j}q_j=\sum_{j\in J}t_{l,j}q_j^*\ \rightarrow\sum_{j\in J}t_{l,j}q_j-\sum_{j\in J}t_{l,j}q_j^*\ =\ 0\rightarrow\ \sum_{j\in J}t_{l,j}q_j\left(\frac{q_j-q_j^*}{q_j}\right)\ =\ 0\rightarrow\sum_{j\in J}t_{l,j}q_j\varsigma_j=0\ \forall l\in\widetilde{L} \tag{9}$$

where $\sum_{j\in J}t_{l,j}q_j=\sum_{j\in J}t_{l,j}q_j^*$ indicates that, with regards to the link choice proportion, the sum of the true and estimated mean OD demand should be equal on observed links. We can break the rightmost side of Eq. (9) to exclude the ς_j belonging to OD demand j:

$$\sum_{j\in J}t_{l,j}q_j\varsigma_j=0\rightarrow\sum_{\substack{j'\in J\\ j'\neq j}}t_{l,j'}q_{j'}\varsigma_{j'}+t_{l,j}q_j\varsigma_j=0\rightarrow\varsigma_j=\frac{-\sum_{\substack{j'\in J\\ j'\neq j}}t_{l,j'}q_{j'}\varsigma_{j'}}{t_{l,j}q_j}\xrightarrow{if\ \varsigma_{j'}\geqslant 1}\varsigma_j^2\leqslant\xi\left(\frac{\sum_{\substack{j'\in J\\ j'\neq j}}t_{l,j'}q_{j'}}{t_{l,j}q_j}\right)^2\xrightarrow{if\ -1\leqslant\varsigma_{j'}\leqslant 1}\left(\frac{\sum_{\substack{j'\in J\\ j'\neq j}}t_{l,j'}q_{j'}}{t_{l,j}q_j}\right)^2 \tag{10}$$

Where in Eq. (10), ξ is a large postive constant. According to Eq. (10), there is an upper bound for each ς_j^2 as long as there is at least one observed link that is traversed by the OD demand j (i.e., $(\exists l\in\widetilde{L}\rightarrow t_{l,j}>0)$. Please note that ς_j^2 is bounded to a finite value if the OD covering rule is met for a sensor location scheme (Yang et al., 1991). With the existence of the upper bound for ς_j^2 , we can derive the upper bound of $\beta_j(s)$ and $\alpha_l(s)$:

$$\alpha_l(s) \leqslant \left(1 - \left(\sum_{k\in K}(F_k(s))x_{k,l}\right)\right)^{-1} \left(\sum_{j\in J} t_{l,j}\left(\frac{\sum_{j'\in J} t_{l,j'}q_{j'}}{t_{l,j}q_j}\right)^2\right) \quad \forall l \in \widetilde{L}, s \in S \quad \text{(I)}$$

$$\beta_j(s) \leqslant \left(1 - \prod_{k\in K}(F_k(s))^{\sum_{l\in L}\widetilde{\varphi_{l,j}}x_{k,l}}\right)^{-1} \left(\frac{\sum_{j'\in J} t_{l,j'}q_{j'}}{t_{l,j}q_j}\right)^2 \quad \forall j \in J, s \in S \quad \text{(II)} \tag{11}$$

The other contributing factors that affect the upper bounds of $\beta_j(s)$ and $\alpha_l(s)$ are related to the failure of sensors. The probability of failure of each sensor type k by time s is $F_k(s)$which is value between 0 and 1. $\prod_{k\in K}(F_k(s))^{\sum_{l\in L}\widetilde{\varphi_{l,j}}x_{k,l}}$ is also a value between 0 and 1. Therefore, if $F_k(s)$in Eq. (11-I) and $\prod_{k\in K}(F_k(s))^{\sum_{l\in L}\widetilde{\varphi_{l,j}}x_{k,l}}$ in Eq. (11-II) is equal to 1 which happens when the failure rate is a relatively large value at time s then there can't be any finite upper bounds for $\beta_j(s)$ and $\alpha_l(s)$. Since the failure of a sensor is not usually a repetitive event in a short period (Salari et al., 2019), however, it is reasonable to assume that sensor failure rate doesn't approach a very large value at time s. This means that neither argument that includes sensor failure rate approaches infinity and that they are thus both bounded within finite upper bounds. Therefore, there exist upper bounds for both $\beta_j(s)$ and $\alpha_l(s)$ as long as the OD covering rule is satisfied. In the following section, we describe the sensor location problem for OD demand estimation in two phases: initial sensor deployment and additional sensor deployment.

5.4. Initial sensor deployment phase

To find the locations of sensors in this phase, we consider the reliability of sensor deployment at a specific time point. For instance, if the sensor deployment occurs at time s, then the objective is to use Eqs. (12) and (13) to minimize the MPIL for OD pairs or for observed links at time s' ($s' > s$), where s' is the choice between overhauling the current sensor deployment and adding additional sensors. We define two categories of objective functions: min–max and min-sum. These serve different purposes in the sensor location problem:

Min-max functions:

$$Z_s^1 = \min_{j\in J}\left(\beta_j(s)\right) \tag{12}$$

$$Z_s^2 = \min_{l\in L}(\alpha_l(s)) \tag{13}$$

where Eqs. (12) and (13) minimize the maximum value of the MPIL on OD pairs or observed links, respectively. In other words, this set of functions addresses the worst-case scenario in terms of MPIL for OD pairs or observed links. An alternative version of Eqs. (12) and (13) is:

Min-sum functions:

$$Z_s^{1'} = min\left(\sum_{j\in J}\beta_j(s)\right) \tag{14}$$

$$Z_s^{2'} = min\left(\sum_{l\in L}\alpha_l(s)\right) \tag{15}$$

Eqs. (14) and (15) are min-sum functions where in Eq. (14) and Eq.(15), the aggregated MPIL for the OD pairs and the aggregated MPIL for the observed links at time s, are minimized. The optimization model lets us select either min–max or min-sum functions, whereupon we can use the unselected objective functions in each category or combine them using either the weighted sums method (WSM) or the ε-constraint method. The WSM can be used to integrate the objective function into a bi-objective function with two components that are weighted to reflect the importance of each component. The ε-constraint method maintains a singular objective function while treating other objective functions as constraints defined as upper or lower bounds, depending on their natures. Both forms of the objective functions obtained with the WSM are shown below:

$$Z_s^{wsm} = min\left(w_1\left(\frac{Z_s^1 - Z_s^{1-Utopia}}{Z_s^{1-Pseudo-nadir} - Z_s^{1-Utopia}}\right) + w_2\left(\frac{Z_s^2 - Z_s^{2-Utopia}}{Z_s^{2-Pseudo-nadir} - Z_s^{2-Utopia}}\right)\right) \quad \text{I}$$

$$Z_s^{wsm'} = min\left(w_1\left(\frac{Z_s^{1'} - Z_s^{1'-Utopia}}{Z_s^{1'-Pseudo-nadir} - Z_s^{1'-Utopia}}\right) + w_2\left(\frac{Z_s^{2'} - Z_s^{2'-Utopia}}{Z_s^{2'-Pseudo-nadir} - Z_s^{2'-Utopia}}\right)\right) \quad \text{II} \tag{16}$$

where Eq. (16-I) addresses the combination of min–max functions and Eqs. (12), (13), and (16-II) use the min-sum functions in a bi-objective formulation. w_1&w_2 ($w_1 + w_2 = 1$) are the weights that convey the importance of the first objective function (Z^1 or $Z^{1'}$) and the second objective function components (Z^2or $Z^{2'}$), respectively. The values of these weights can be determined using expert judgment, by the reliability of the information gain, or by considering the primary purpose of the sensor installation. The objective function components, Eqs. (12) and (13) or Eqs. (14) and (15), are normalized in Eq. (16) using a utopia point and pseudo-nadir points.

In Eq. (16-I), $Z_s^{1-Utopia}$ and $Z_s^{2-Utopia}$ are the utopia points for the first and second objective function components, respectively. The pseudo-nadir points of these objective function components, $Z_s^{1-Pseudo-nadir}$ and $Z_s^{2-Pseudo-nadir}$, define the worst feasible solutions using the decision variables'[9] feasible values. Similar to Eq. (16-I), Eq. (16-II) uses the utopia and nadir points of the first and the second objective function components introduced in Eqs. (14&15) to normalize these functions.

The ε-constraint method uses either the first objective function component (Z^1 or$Z^{1'}$) or the second objective function component (Z^2 or $Z^{2'}$) as the main objective function with the other objective function component redefined as a constraint. Thus, there are four possible outcomes for the objective function:

	I		II
MIN-MAX FUNCTION	$Z_s^{\varepsilon-constra\,int} = Z_s^1 = \min_{j\in J}\left(\beta_j(s)\right)$		$Z_s^{\varepsilon-constra\,int} = Z_s^2 = \min_{l\in\widetilde{L}^0}\left(\alpha_l(s)\right)$
	$s.t.,$	OR	$s.t.,$
	$Z_s^2 \le \partial_s^2$		$Z_s^1 \le \partial_s^1$
	III		IV
MIN-SUM FUNCTIONS	$Z_s^{'\varepsilon-constra\,int} = Z_s^{1'} = \min\left(\sum_{j\in J}\beta_j(s)\right)$		$Z_s^{'\varepsilon-constra\,int} = Z_s^{2'} = \min\left(\sum_{l\in\widetilde{L}^0}\alpha_l(s)\right)$
	$s.t.,$	OR	$s.t.,$
	$Z_s^{2'} \le \partial_s^{2'}$		$Z_s^{1'} \le \partial_s^{1'}$

(17)

where the objective functions are divided between min-sum or min–max functions. ∂^1 and ∂^2 are the upper bound boundaries for Z^1 and Z^2, respectively. In the other segments of Eq. (17), $\partial_s^{1'}$ and $\partial_s^{2'}$ are also the upper bound boundaries for $Z^{1'}$ and $Z^{2'}$. Note that the values of upper bound boundaries can contribute to the optimization problem's feasibility. We must therefore meticulously determine these values to avoid having the optimization problems defined in Eq. (17) become infeasible. We can achieve this by solving one of the optimization forms of Eq. (17) so we may use the optimal value as the upper bound of the constraint as we change the objective function. In addition to the WSM and ε-constraint related constraints, other general constraints should be employed for both methods, including the budget constraint (Eq. (18)), the sensor deployment constraint (Eq. (19)), the OD covering rule (Eq. (20)), and the constraints associated with the relationship between the true and estimated mean OD demands on the observed links (Eq. (21)).

$$\sum_{k\in K}\sum_{l\in L} c_k x_{k,l} \leqslant \eta \tag{18}$$

$$\sum_{k\in K} x_{k,l} = 1 \ \forall l \in \widetilde{L} \tag{19}$$

$$\sum_{l\in L}\sum_{k\in K} \varphi_{l,j} x_{k,l} \geqslant 1 \ \forall j \in J \tag{20}$$

$$\sum_{j\in J} t_{l,j} q_j - \sum_{j\in J} t_{l,j} q_j^* = \sum_{j\in J} t_{l,j} q_j \left(\frac{q_j - q_j^*}{q_j}\right) = 0 \rightarrow \sum_{j\in J} t_{l,j} q_j \varsigma_j = 0 \ \forall l \in \widetilde{L} \tag{21}$$

where η is the budget constraint that restricts the number of sensors installed on the links in the network in Eq. (18). The budget in this

[9] For more information on pseudo-nadir points and utopia points, please refer to Appendix B.

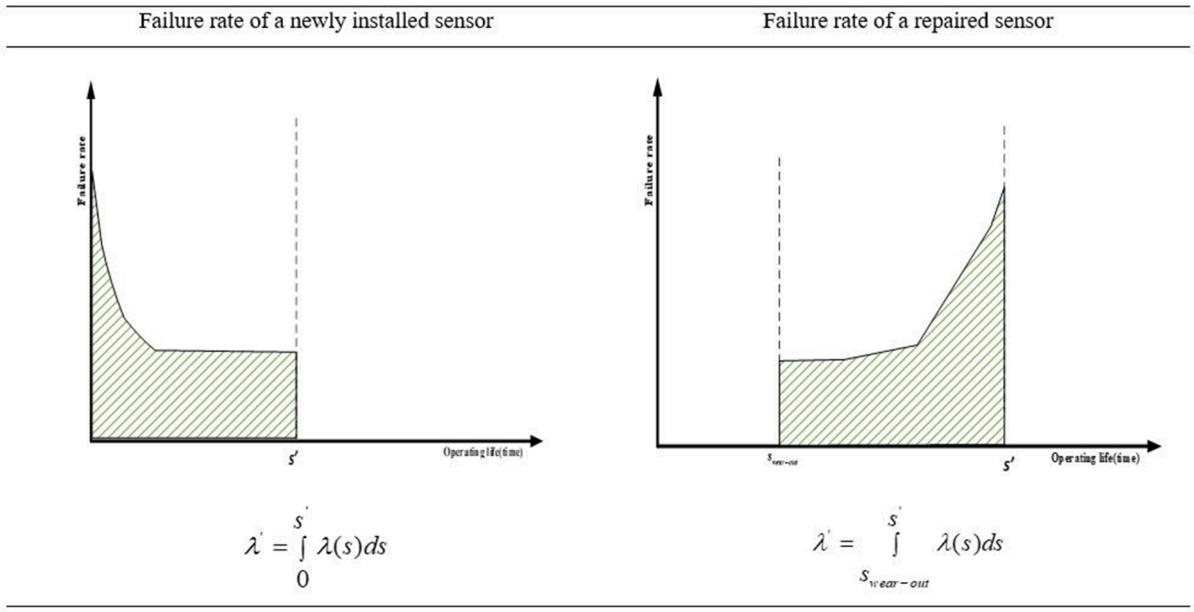

Fig. 6. The failure rate of repaired sensor (left) and a newly installed sensor (right) at the additional sensor deployment phase.

study also constrains the types of sensors that can be deployed on links, where a larger budget supports the installation of more advanced sensors with lower probabilities of failure. Eq. (19) enforces the rule that only one sensor should be installed on each observed link in a road network. Eq. (20) addresses the OD covering rule, which says that the OD demand of each OD pair should be observed by at least one sensor. Eq. (21) demonstrates that subtracting the sum of the true mean OD demand from the estimated OD demand will result in zero on each observed link $l(\forall l \in \widetilde{L})$. To add ς_j to this equation, we multiply and divide the resulting subtraction by q_j.

5.5. Additional sensor deployment phase

In the additional sensor deployment phase, we can preserve or increase the reliability of the sensor allocation by repairing failed sensors or adding new sensors to the current sensor deployment. For instance, at time s in the additional sensor deployment phase, if the existing sensors have not failed, we must consider whether they are in their wear-in, useful life phase, or wear-out phase. If the existing sensors have already failed by time s, then they can be either repaired or replaced by new sensors. The cost to repair a sensor of type k, $c_k^{'}$, is assumed to be less than the cost of installing a new sensor of the same type, i.e., $c_k^{'} < c_k \ , \forall k \in K$. It is assumed that the failure rate of a repaired sensor continues to follow the same time-dependent failure rate as the wear-out phase. In other words, a repaired sensor's failure rate is still higher than that of a newly-deployed sensor. When the additional sensor deployment phase occurs at time s, the objective is to minimize the MPIL for OD pairs or observed links at time $s^{'}$ $(s^{'} > s)$ where time $s^{'}$ is considered the time when the current sensor deployment will be subject to routine inspection.

Fig. 6 shows two instances of failure rate curves at time s: one for a newly installed sensor and one for a repaired sensor. The graph on the left illustrates a new sensor installation at time s, with the failure rate curve following the wear-in, useful life, and wear-out phases. A sensor that is newly-installed at time $s$begins its service life at time *zero* of its time-dependent failure rate function. The parameter of the Poisson distribution for this sensor at a future time $s^{'}$ is equal to the area under the curve from time zero to $s^{'}$ (shown as the dashed green area under the curve on the left). The right side of the Figure demonstrates the situation where a sensor is repaired at time s and the updated failure rate of the sensor follows the wear-out phase. This means that the sensor repaired at time s starts working at the beginning of its wear-out phase, which is represented in Fig. 6 by $s_{wear-out}$. The parameter of the Poisson distribution for this sensor at a time $s^{'}$ is equal to the area under the curve between time $s_{wear-out}$ and $s^{'}$ (shown as the dashed green area under the curve on the right).

In the additional sensor deployment phase, new sensors can also be installed on links that were not previously equipped with any sensors during the initial sensor deployment phase. The locations of these sensors can be determined using Eqs. (16) and (17), which were introduced in Section 5.4, as the objective functions. Placing additional sensors can minimize the adverse effect of a likely future sensor failure at time $s^{'}$ where $s^{'} > s$. In addition, deploying additional sensor can help in providing a better OD demands estimation.

To decide where to deploy new sensors and/or repair existing sensors at time s, the constraints introduced for initial sensor deployment must be modified. This modification includes an updated budget constraint, the type of sensors that are available to be deployed, an updated OD covering rule with consideration for existing sensors and new installations or repaired sensors. To be more

specific, Eq. (22) enforces the budget constraint for the deployment of new sensors and/or the repair of failed sensors, where $\eta^{'}$ is the budget cap. In this equation, $x^{'}_{k,l}$ is a binary variable that determines whether a sensor of type k is installed on link l at the additional sensor deployment phase, and $y^{'}_{k,l}$ is a binary variable that determines whether a failed sensor installed on link l should be repaired. According to Eq. (23), one sensor should be installed on each observed link ($\forall l \in \widetilde{L}^{'}$) at the additional sensor deployment phase, where $\widetilde{L}^{'}$ represents the set of links equipped with new sensors at this phase. Eq. (24) addresses the OD covering rule, which implies that the OD demand of each OD pair should be observed by at least one sensor at time s. This observation could be from the existing sensors, $\vartheta_{l,s} = 1$, or from the sensors installed or repaired during the additional sensor deployment phase. Eq. (25-I) dictates that if a sensor was installed on link l during the initial deployment phase, i.e., $\forall l \in \widetilde{L}$ and is still working at time s, i.e., $\vartheta_{l,s} = 1$, then the sensor on this link cannot be repaired and no additional sensors should be installed at that location during the additional sensor deployment phase. Eq. (25-II) determines that if link l is not an observed link at the initial sensor deployment phase, i.e., $\forall l \notin \widetilde{L}$, then the binary variable corresponding to the repair of sensor type k on link l, i.e., $y^{'}_{k,l}$, should be zero. Eq. (26) demonstrates that there are two circumstances under which subtracting the sum of the true mean OD demand from the estimated OD demand on a link will result in zero: Where a link is instrumented with a sensor during the initial sensor deployment phase and still works at time s; and where a link is equipped with a sensor or having a sensor repaired during the additional sensor deployment phase. Note that in this Equation, $q^{'}_{j}$ is the estimated OD demand for OD pair j during the additional sensor deployment phase.

$$\sum_{k\in K}\sum_{l\in \widetilde{L}} c^{'}_{k} y^{'}_{k,l} + \sum_{l\in L} c_k x^{'}_{k,l} \leqslant \eta^{'} \tag{22}$$

$$\sum_{k\in K} x^{'}_{k,l} = 1 \ \forall l \in \widetilde{L}^{'} \tag{23}$$

$$\sum_{l\in \widetilde{L}\cup L}\sum_{k\in K} \varphi_{l,j}(x^{'}_{k,l} + \vartheta_{l,s} + y^{'}_{k,l}) \geqslant 1 \ \forall j \in J, s \in S \tag{24}$$

$$\begin{aligned} x^{'}_{k,l} \ + \ y^{'}_{k,l} &\leqslant 1 - \vartheta_{l,s} \ \forall l \in \widetilde{L}, k \in K, s \in S \quad \text{(I)} \\ y^{'}_{k,l} &= 0 \ \forall l \in L\backslash\widetilde{L}, k \in K \quad \text{(II)} \end{aligned} \tag{25}$$

$$\begin{aligned} &\sum_{j\in J} \vartheta_{l,s} t_{l,j} q^{'}_{j} - \sum_{j\in J} \vartheta_{l,s} t_{l,j} q^{*}_{j} \ = \ \sum_{j\in J} t_{l,j} q_j \vartheta_{l,s} \left(\frac{q^{'}_{j} - q^{*}_{j}}{q^{'}_{j}}\right) \ = \ 0 \rightarrow \sum_{j\in J} \vartheta_{l,s} t_{l,j} q^{'}_{j} \varsigma_j = 0 \ \forall l \in \widetilde{L}, s \in S \quad \text{(I)} \\ &\sum_{j\in J} t_{l,j} q^{'}_{j} - \sum_{j\in J} t_{l,j} q^{*}_{j} \ = \ \sum_{j\in J} t_{l,j} q^{'}_{j} \left(\frac{q^{'}_{j} - q^{*}_{j}}{q^{'}_{j}}\right) \ = \ 0 \rightarrow \sum_{j\in J} t_{l,j} q^{'}_{j} \varsigma_j = 0 \ \forall l \in \widetilde{L}^{'} \text{ or } l \in \widetilde{L} \ \& y^{'}_{k,l} = 1 \quad \text{(II)} \end{aligned} \tag{26}$$

6. Solution algorithm

In this section, we describe the solution algorithm used in this study. This includes explanations of the random link choice proportion and the Genetic Algorithm (GA) that were employed to solve the proposed model.

6.1. Description of the OD estimation process with a stochastic link choice proportion

We assume that the link choice proportion inherits stochastic behavior and must be updated through the estimation process. We use the maximum entropy (ME) method to estimate the OD demands from the observed link flows that were obtained from the assigned sensors[10]. Note that, depending on the availability of prior OD information and associated traffic data, other OD estimation methods such as Bayesian estimation, generalized least square, or maximum likelihood can be used in place of ME[11]. Eqs. (27) and (28) present the ME formula for OD estimation (Van Zuylen and Willumsen, 1980):

$$Z_{ME} = max \left(- \sum_{j\in J} q_j \left(ln \frac{q_j}{q_j^{prior}} - 1 \right) \right) \tag{27}$$

s.t.,

[10] For more information on the model formulas related to ME, please refer to Van Zuylen and Willumsen (1980).

[11] Note that the choice of the functional form of the OD demand estimation method might affect the optimal sensor location results; more research should be conducted to investigate this impact.

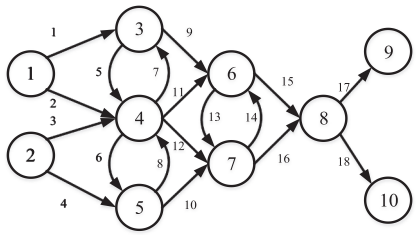

Fig. 7. Fishbone network.

Table 6
OD details of the Fishbone network.

OD#	OD nodes	Routes	Prior OD demand (pcu/hr)
1	1–9	{1,9,15,17} {2,11,15,17}	200
2	1–10	{1,9,15,18} {2,7,9,15,18}	350
3	2–9	{3,12,14,15,17} {2,6,10,16,17}	250
4	2–10	{4,8,12,16,18}	510

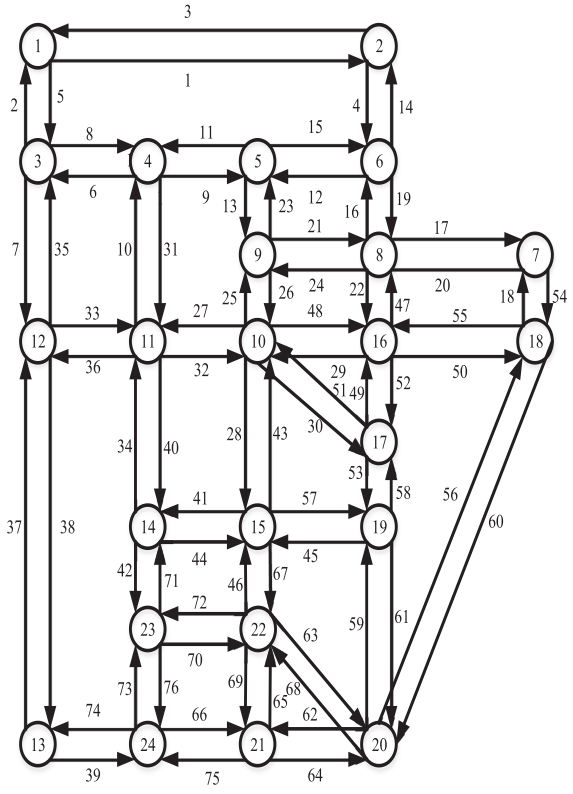

Fig. 8. Graphical illustration of Sioux Falls network.

$$v_l = \sum_{j \in J} t_{l,j} q_j \ \forall l \in \widetilde{L} \tag{28}$$

Using the SUE, we can update the link flows and the link choice proportion with the estimated OD demands. To solve the SUE, we employ the Frank-Wolfe algorithm, which is an iterative first-order optimization algorithm for constrained convex formulas (Fukushima, 1984). The information obtained from the SUE should be consistent with the observed link flows and link choice

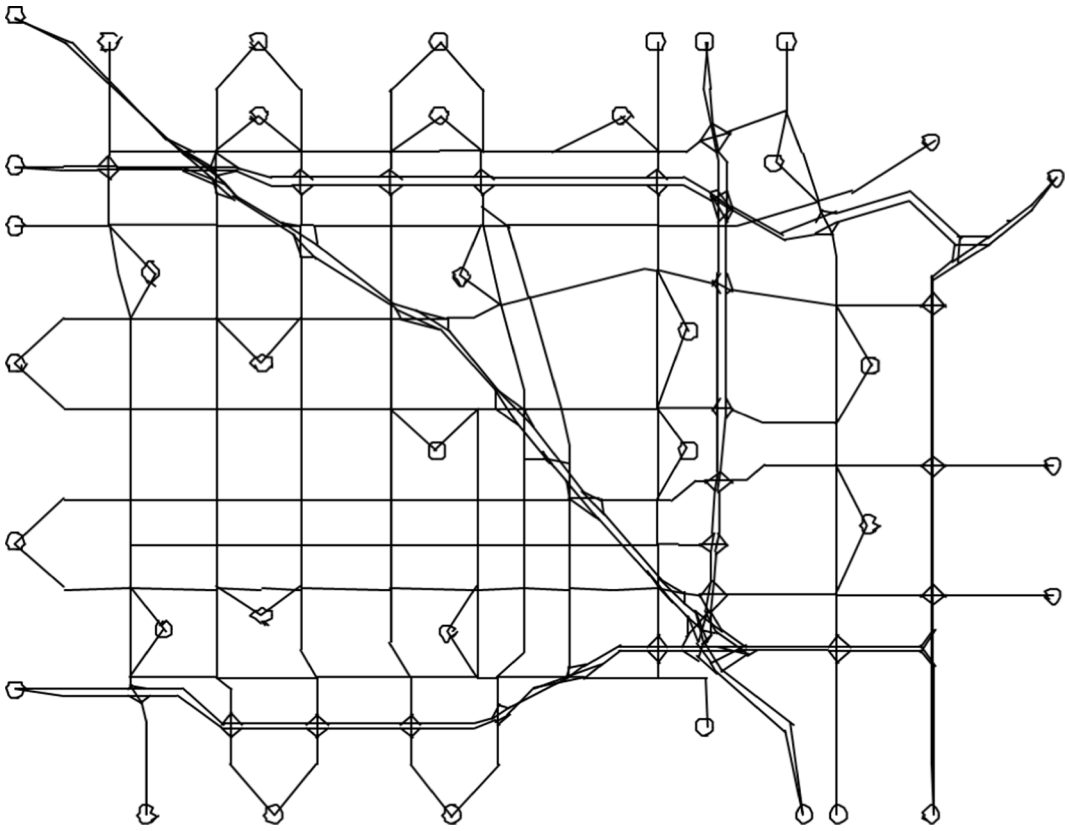

Fig. 9. Graphical illustration of Anaheim network.

proportions. Thus, we set the Frank-Wolfe algorithm to be updated iteratively until the difference between the estimated link flows obtained from the traffic assignment and observed link flows obtained from traffic counts is less than the tolerance rate, which in this case is set to 0.001. With the estimated OD values and the updated link choice proportion, we can use the proposed model to calculate the OD demand information gain from the current sensor assignment and, if required, update the assignment process to maximize the information gain.

6.2. Genetic algorithm (GA)

To solve the optimization problems presented in sections 5.4 and 5.5, we used a genetic algorithm (GA) specifically designed for each problem. The output of the GA determines the location of sensors and the type of sensor to be deployed at each location at the initial and additional sensor deployment phases. We explained the details of the proposed GA in Appendix C.

7. Numerical examples

This section details the implementation of the proposed model for three illustrative example networks: The Fishbone network and the Sioux Falls network and the Anaheim network. All of these networks have been frequently used in previous related studies (Ng, 2012, 2013; Hu and Liou, 2014; Xu et al., 2016; Salari et al., 2019).

Fishbone network: The Fishbone network is small, with six non-centroid nodes and four centroid nodes. Nodes 1 and 2 are origin nodes and nodes 9 and 10 are destination nodes. The network has eighteen links that connect the origin nodes to destination nodes. An illustration of the Fishbone network is shown in Fig. 7.

Table 6 shows information related to the Fishbone network's OD nodes, the routes between each OD pair, and the network's prior OD flows. According to this table, this network has four OD pairs between origin nodes and destination nodes. The prior OD[12] demand information for each OD pair, in which the OD demands are converted to passenger car units per hour (pcu/hr), is also shown. Note that this information is randomly generated rather than coming from a real data source. The remainder of the information related to

[12] Readers can refer to the Section 8.9.1 of the book entitled "Transportation System Analysis: Models and Applications" by Ennio Cascetta (2009) for more information on methods used to determine prior OD demand estimations.

Table 7
Information about two sensor types.

Sensor type	time-dependent failure rate function	Cost per sensor (×100$)	Repair cost per sensor (×100$)
1 (Basic)	$\lambda_1(s) = \begin{cases} 4 - s^2 & 0 \leqslant s < 1 \\ 3 & 1 \leqslant s < 4 \\ s^2 - 13 & s \geqslant 4 \end{cases}$	120	60
2 (Advanced)	$\lambda_2(s) = \begin{cases} 3 - s & 0 \leqslant s < 1 \\ 2 & 1 \leqslant s < 6 \\ s - 4 & s \geqslant 6 \end{cases}$	180	90

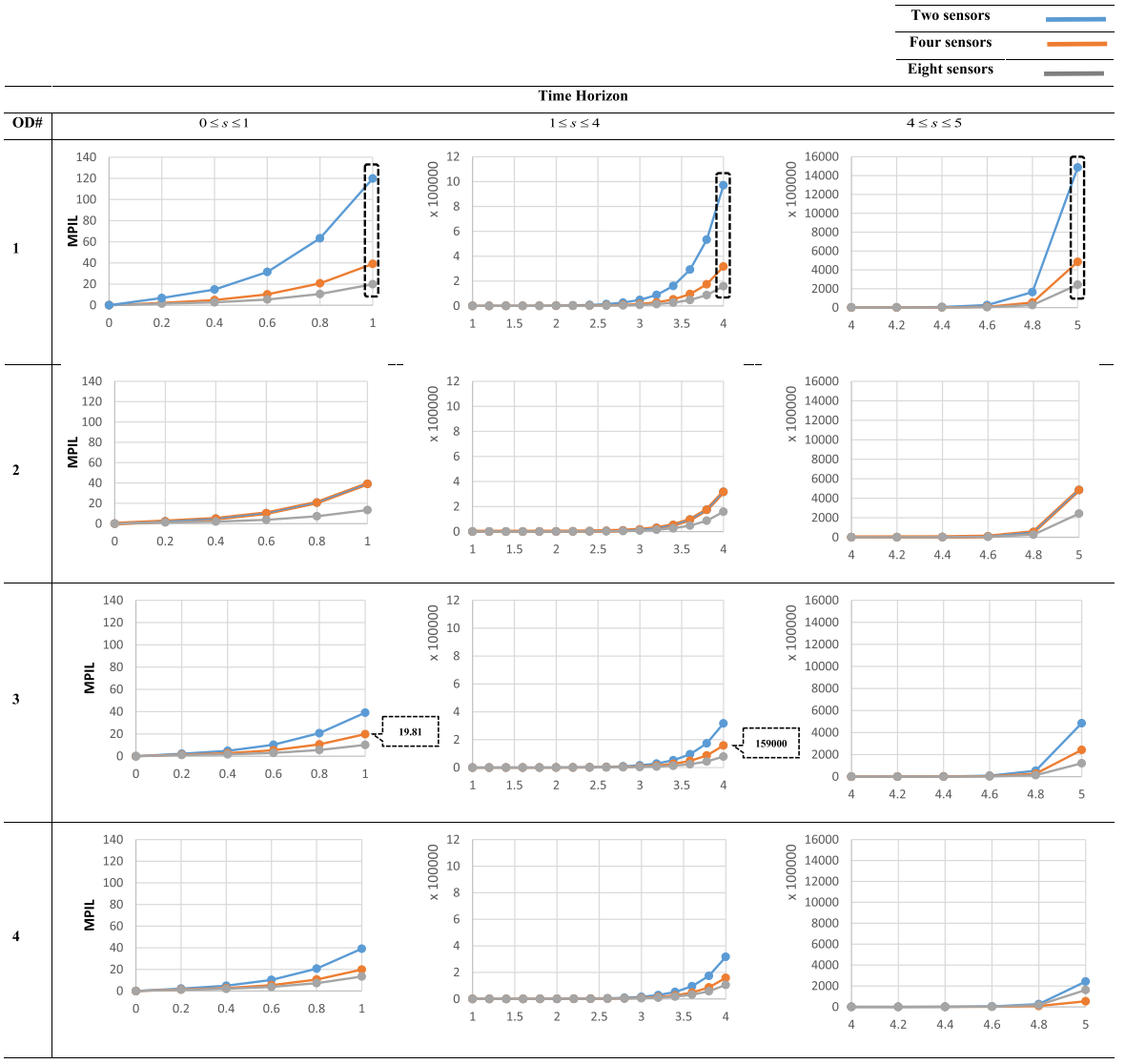

Fig. 10. Sensitivity of the OD demand flow information loss to the number of sensors.

this network, including the link flows and link choice proportions, can be found in Appendix D.

Sioux Falls network: The mid-sized Sioux Falls network, which consists of 76 links and 24 nodes, is representative of the city of Sioux Falls, South Dakota, United States. Consistent with Fu et al. (2019), we assume that there are 30 OD pairs in this network. An illustration of the Sioux Falls network is shown in Fig. 8. Information related to OD nodes, prior OD demand, and true OD demand can be found in Appendix E.

Table 8
MPIL on OD pairs at time $s = 5$.

Budget	Set of observed links		MPIL on OD pairs ($\times 10^6$)				
	Basic	Advanced	1	2	3	4	Aggregated
400	{1,16,17}	–	242.6	485.2	386.5	485.2	1599.5
500	{6}	{15,16}	0.111	0.036	0.019	0.036	0.202
600	{3,16}	{2,18}		0.038	0.054	0.036	0.164
750	–	{1,15,16,17}		0.018	0.012		0.102

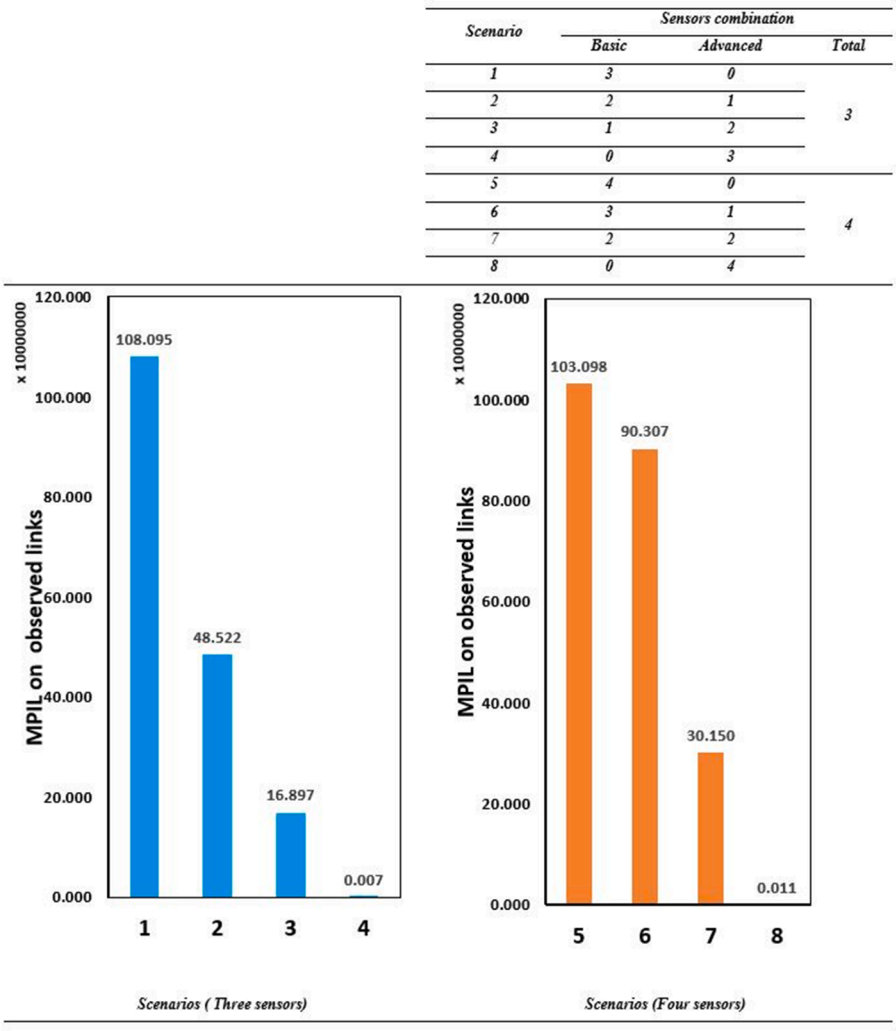

Fig. 11. Average MPIL on observed links.

Anaheim network: The large Anaheim road network is based on the city of Anaheim, which is located outside Los Angeles in Southern California, United States. A graphical illustration of the city is depicted in Fig. 9. The network consists of 416 nodes, 914 links, and 1,406 OD pairs. Information about this road network is from Oh and Jayakrishnan (2002)[13]. To generate all possible routes from origin to destination, we used the K-shortest path algorithm initially proposed by Yen (1970) and assumed there are three paths between each OD pair. This results in 4,218 routes between all OD pairs.

We assume that there are two available sensor types: basic and advanced. Both types are assumed to be from the counting sensor category. Table 7 shows detailed information about the differences between the two sensor types, including their costs and their time-

[13] The attributes of this network can be found at https://www.bgu.ac.il/~bargera/tntp/

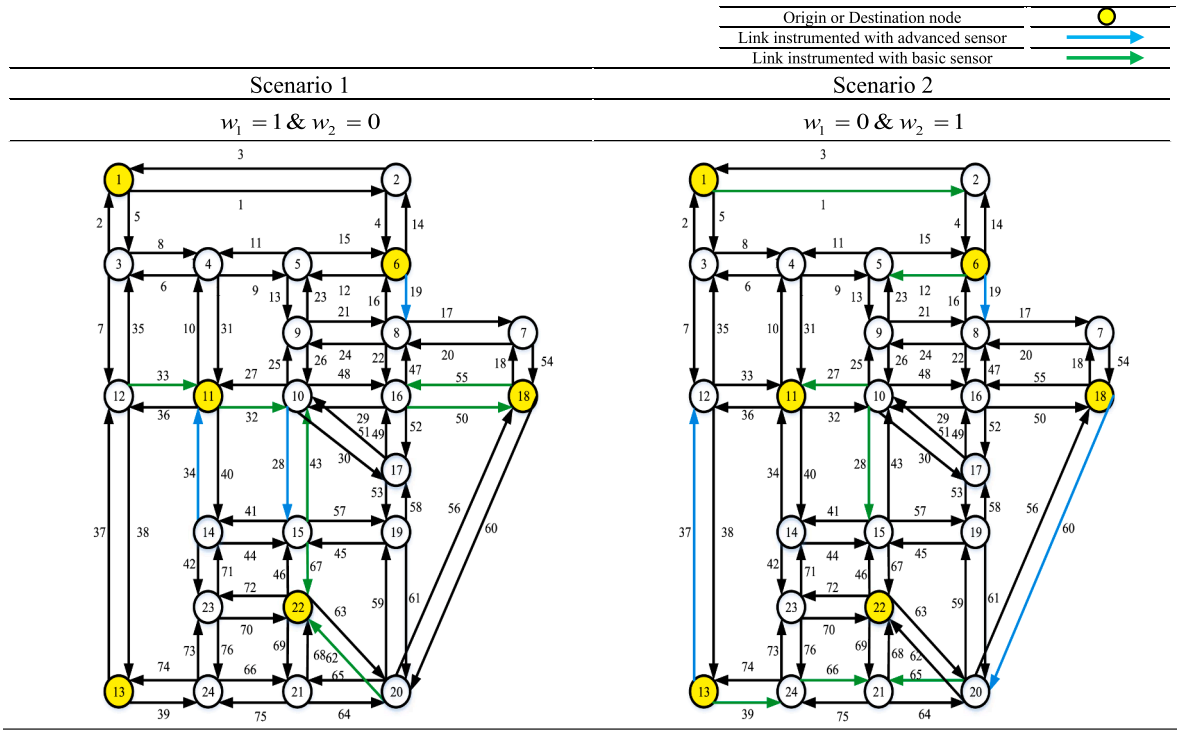

Fig. 12. Location of advanced and basic sensors in the Sioux Falls network.

dependent failure rates during their wear-in, useful life, and wear-out phases. According to Table 7, the basic sensor has a higher failure rate per given period than the advanced sensor, but it is less expensive. For both sensor types, it is assumed that the failure rates decrease over the duration of the wear-in phase, remain constant throughout the useful life phase, and then increase during the wear-out phase. Note that the failure rates introduced in Table 7 are for illustrative purposes and can be defined more realistically by leveraging the historical data of the failure rates of real-life sensors. The dollar amounts shown in the "Cost per sensor" column are assumed to include both purchase price and installation costs.

We performed a series of experiments to address the following questions:

Section 7.1: What effect do the number and type of sensors have on the MPIL for OD pairs and observed links during the initial sensor deployment phase?
Section 7.2: How can the reliability of sensor deployment be assessed to support a additional sensor deployment phase and how can the best locations for additional sensors be identified?
Section 7.3: What is the convergence rate of the proposed GA for different network sizes?

7.1. Initial sensor deployment phase:

We implemented initial sensor deployments for the Fishbone and Sioux Falls networks. The initial sensor deployment for both networks is assumed to occur at time $s = 0$ and the overhaul/maintenance of the sensor deployment is assumed to occur at time $s = 5$. In other words, the purpose of sensor deployment at this phase is to minimize the MPIL for OD pairs/observed links at times $= 5$.

7.1.1. Impact of the number of sensors on MPIL for OD pairs: Fishbone network

For time $0 \leqslant s \leqslant 5$, Fig. 10 assesses the effect of the number of sensors on the MPIL for each OD pair in the Fishbone network, assuming that all sensors in the network are identical[14]. The number of basic sensors ranges from two to eight, with two sensors being the minimum amount necessary to satisfy the OD covering rule. We use Eq. (17-III), as the single objective function to initially locate the sensors. There is no upper bound for the maximum demand flow information loss on links.

The vertical axis in Fig. 10 represents the MPIL of OD pairs and the horizontal axis demonstrates the time horizon, which is divided into three segments: $0 \leqslant s \leqslant 1$, $1 \leqslant s \leqslant 4$, and $4 \leqslant s \leqslant 5$. The first time segment, $0 \leqslant s \leqslant 1$, belongs to the wear-in phase where the failure rate of

[14] All sensors are assumed to be basic sensors.

Table 9
Different possible failure scenario for installed sensors in Fishbone network in additional sensor deployment phase.

Initial sensor deployment		Failed sensor by times = 5	Repaired sensor	newly installed sensor	
Basic	Advanced			Basic	Advanced
{1,16,17}	–	{16}	{16}	–	{4}
		{1,17}	{17}		{9}
		{1,16,17}	{17}		{18}
{12,16}	{2}	{12}	{12}	–	{18}
		{2,16}	{2,16}	{18}	–
		{2,12,16}	{2}	–	{18}
{6}	{15,16}	{6}	{6}		{11}
		{6,15}	{6,15}	{11}	–
		{6,15,16}	{6,15,16}	–	

sensors decreases over time. The second time segment, $1 \leqslant s \leqslant 4$, corresponds to the useful life phase. The final time segment, $4 \leqslant s \leqslant 5$, is the wear-out phase. Comparing the MPIL for a certain number of sensors across different time segments demonstrates that the value of the MPIL is considerably higher in the wear-out phase than in a sensor's useful and wear-in phase. For a certain number of sensors, a similar observation can be seen when comparing the MPILs of OD pairs in the useful life and wear-in phases. For instance, in the Fishbone network, the MPIL of the third OD pair at time $s = 1$with four sensors deployed is 19.81. This value increases to 159,000 at time $s = 4$ for the same number of sensors.

Regarding the effect of the number of sensors on the MPIL, we can observe that the MPIL for each OD pair drops considerably while the number of sensors increases. For instance, the first OD pair's MPIL is at its lowest value for all time segments when there are eight sensors installed in the Fishbone network. It is also noteworthy that the number of observed links that are traversed by the second OD pair is equal when there are two or four sensors deployed.

7.1.2. Impact of the different sensor type on MPIL for OD pairs and observed links: Fishbone network

Table 8 describes the MPIL for each OD pair at time $s = 5$. With the objective function set as Equation (17-III), the model determines the type and number of sensors from the two types of available sensors described in Table 7 (i.e., basic and advanced sensors) to be installed in the Fishbone network for different budget constraints. According to Table 8, each OD pair's MPIL decreases when the budget increases. In general, as the ratio of advanced sensors to basic sensors increases, the MPIL of the OD pairs decreases, with a more noticeable decrease for links that become instrumented with advanced sensors. For instance, when the budget is set at 500 (× \$100), OD #4 witnesses a significant reduction in its MPIL compared to the case corresponding to a budget constrain of 400 (× \$100). From the set of links traversed by this OD pair including links 4, 8, 12, 16, and 18, link 16 is instrumented with only a basic sensor when the budget constraint is set at 400(× \$100). However, as the budget constraint increases to 500(× \$100), link 16 becomes equipped with an advanced sensor. The deployment of an advanced sensor on link 16 explains the notable reduction in MPIL of the fourth OD pair.

Fig. 11 shows an evaluation of the MPIL for the observed links at time $s = 5$ for the different combination of basic and advanced sensors. We divided this Figure into two segments, where the image on the left shows the MPIL on observed links for the sensor combination scenarios (i.e., scenarios 1, 2, 3 and 4) that include three sensors in total. The image on the right illustrates the MPIL for observed links for the sensor combinations that include four sensors in total. The bars on each side of Fig. 11 show the cumulative MPIL for the observed link divided by the number of sensors, i.e., the average MPIL for the observed links. Fig. 11 demonstrates that using the objective function to minimize the MPIL for OD pairs can also positively affect the MPIL for observed links. For instance, we can see by comparing the figures that the average MPIL for the observed link decreases as the number of sensors increases.

Fig. 11 supports using the objective function to minimize the MPIL for OD pairs by demonstrating that it can also reduce the MPIL for observed links. In the following section, we will study sensor location deployment using two distinctive objective functions. Our goal is to minimize the MPIL for OD pairs and for observed links so we can explore whether both objective functions generally recommend the same sensor location deployment.

7.1.3. Impact using different objective functions on the sensor location: Sioux Falls network

We implemented the proposed model for the Sioux Falls network using two scenarios where the weights of the objective functions introduced in Eq. (16-I) were either $w_1 = 1 \& w_2 = 0$ or $w_1 = 1 \& w_2 = 0$. Fig. 12 shows the results for each of these scenarios. It is assumed that three advanced sensors and seven basic sensors can be installed in the Sioux Falls network. In Scenario 1, where $w_1 = 1 \& w_2 = 0$, the model focuses on minimizing the OD pairs' MPIL. The estimated OD demand values show that OD pairs 6–18[15], 6–22, 18–22, 22–11, 11–22, and 13–22 inherit the highest OD demands in this network. The links instrumented with advanced sensors in Scenario 1, therefore, are the links traversed by the OD demands of these OD pairs to minimize these OD pairs' maximum MPIL values. In Scenario 2, where $w_1 = 0 \& w_2 = 1$, the model attempts to minimize the maximum MPIL value on its links such that the links with the highest flows (links 37, 60, and 19) are instrumented with the advanced sensors. In the real map of Sioux Falls, these links are associated with parts Highways 29 and 229, which typically carry heavier traffic loads compared to other arterials.

[15] This notation means that node 6 is the origin node and node 18 is the destination node

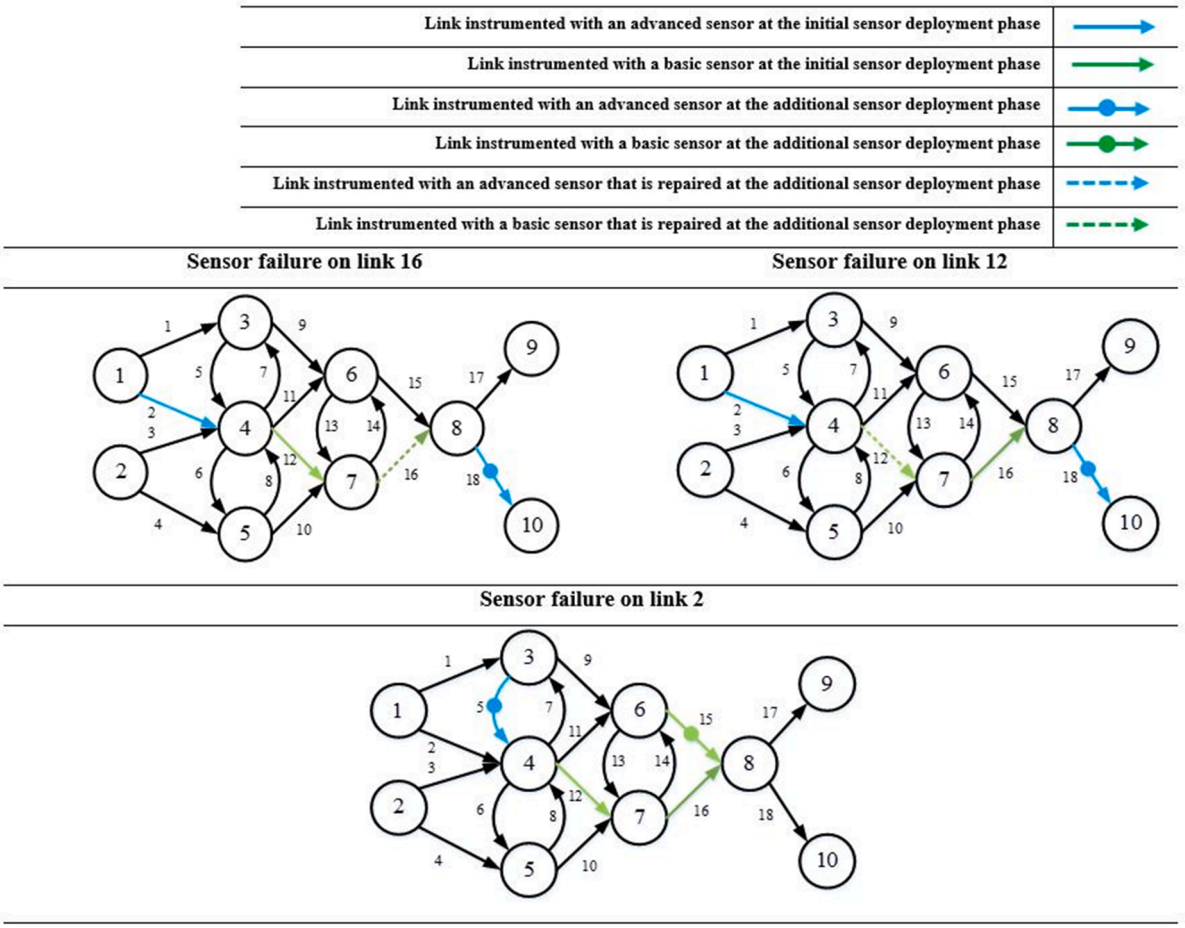

Fig. 13. Location of advanced and basic sensors in the Fishbone network.

7.2. Additional sensor deployment phase:

We evaluated an additional sensor deployment phase for the Fishbone and Sioux Falls networks. For both networks, it is assumed that the additional sensor deployment occurs at time $s = 5$ and that the next scheduled maintenance occurs at $s = 10$. The purpose of the additional sensor deployment phase is to minimize the MPIL for OD pairs/observed links at time $s = 10$ by adding new sensors at optimized locations and repairing or replacing failed sensors.

7.2.1. Additional sensor deployment concerning MPIL for OD pairs: Fishbone network

Table 9 shows the locations of new sensors and highlights the decision to either repair or replace failed sensors during the additional sensor deployment phase. These results are achieved using Eq. (17-I) as the objective function. Table 9 assumes that three sensors are initially installed in the Fishbone network using the combination of advanced and basic sensors shown in Fig. 11. The budget is assumed to be 280 ($\times$ \$100). In each row of Table 9, the column entitled "Failed sensor by time $s = 5$" shows one of possible sensor failure scenarios by time $s = 5$. For instance, the Table's first row shows a scenario where three basic sensors were installed on links 1, 16, and 17 during the initial sensor deployment phase. The failure of the sensor installed on link 16 is considered as one of the possible sensor failure scenarios. According to Table 9, the solution for the additional sensor deployment phase is for the failed sensor on link 16 to be repaired and one new advanced sensor to be installed on link 4.

The results shown in Table 9 indicate that the proposed model favors the deployment of advanced sensors over basic sensors as new sensors. On some occasions, the deployment of new advanced sensors is even favored over the repair of existing sensors if it is achievable within the budget constraint. For instance, in the scenario where all three basic sensors installed on links 1, 16, and 17 are assumed to fail by time $s = 5$, the proposed model suggests repairing the sensor installed on link 17 and deploying a new advanced sensor on link 18 instead of repairing the other two failed sensors.

Fig. 13 shows the evaluation of different sensor failure scenarios where links 12 and 16 are instrumented with basic sensors and link 2 is equipped with an advanced sensor during the initial sensor deployment phase. This sensor combination is listed in Table 9, although this Table only outlines one sensor failure scenario, where one of the three sensors is assumed to fail by time $s = 5$. Fig. 13

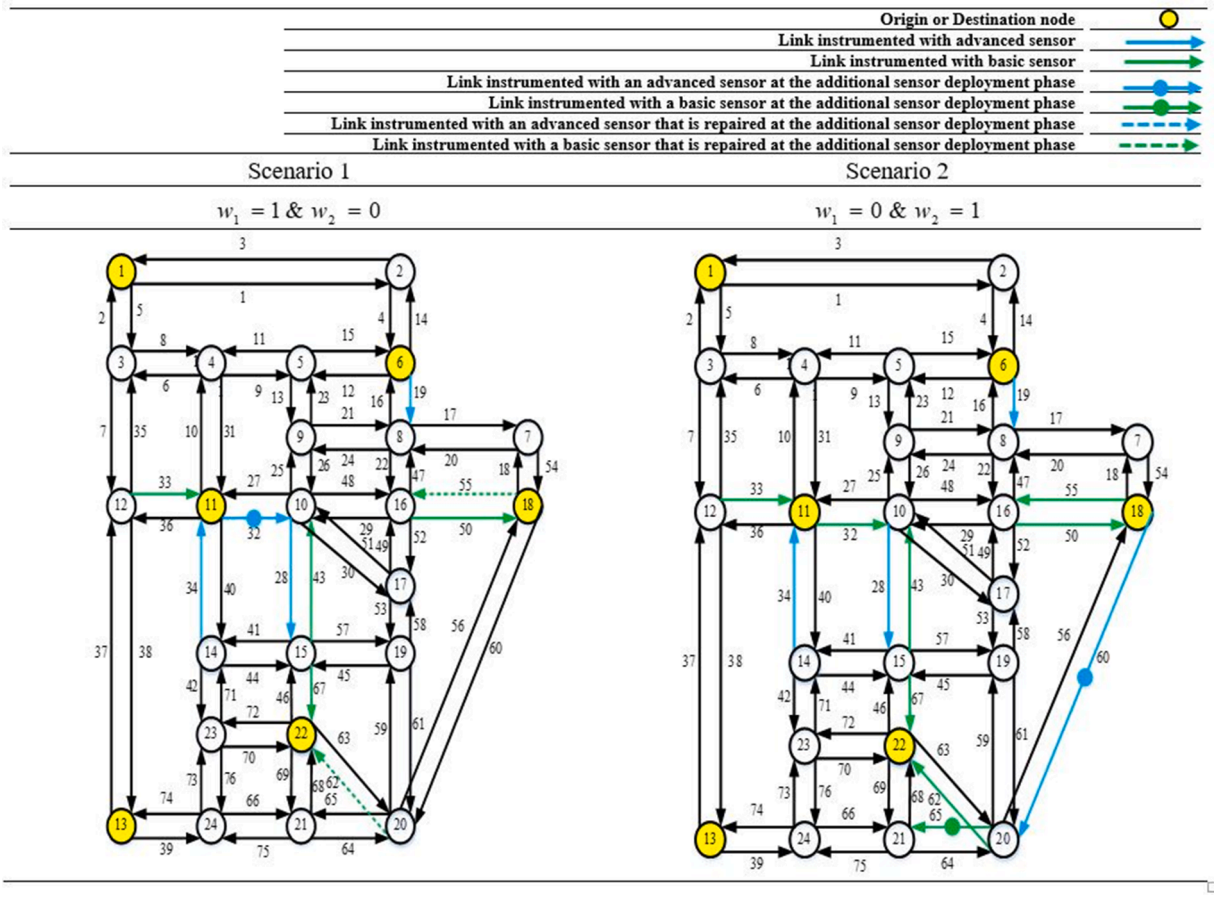

Fig. 14. The effect of objective function weights on the sensor repair/allocation at the additional sensor deployment phase.

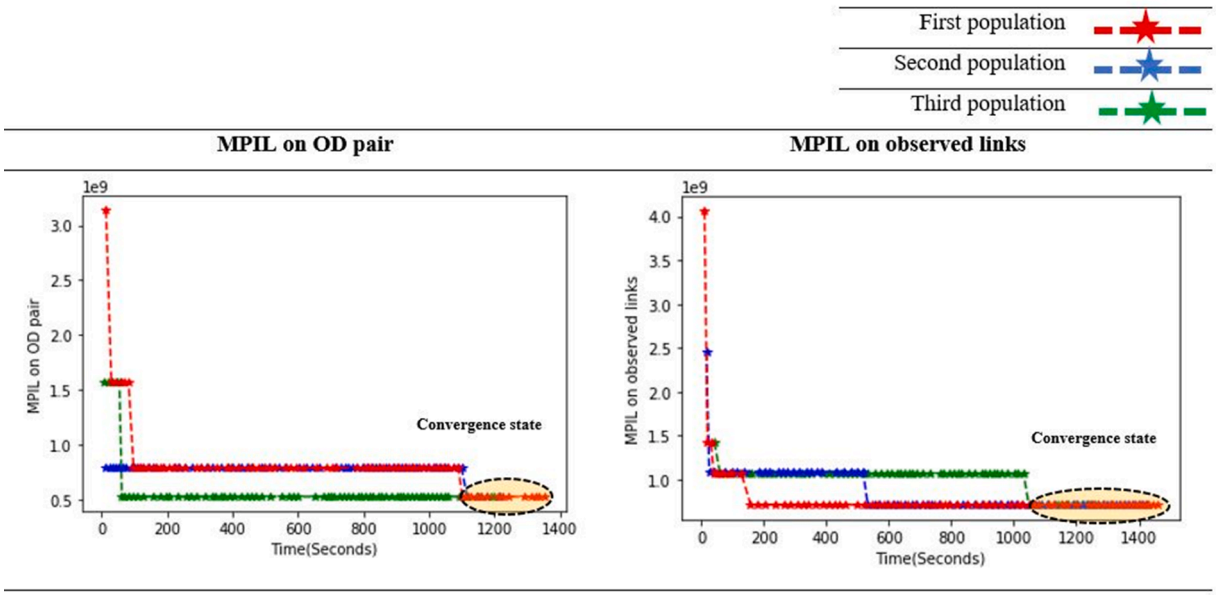

Fig. 15. Pattern of the GA for the Sioux Falls network.

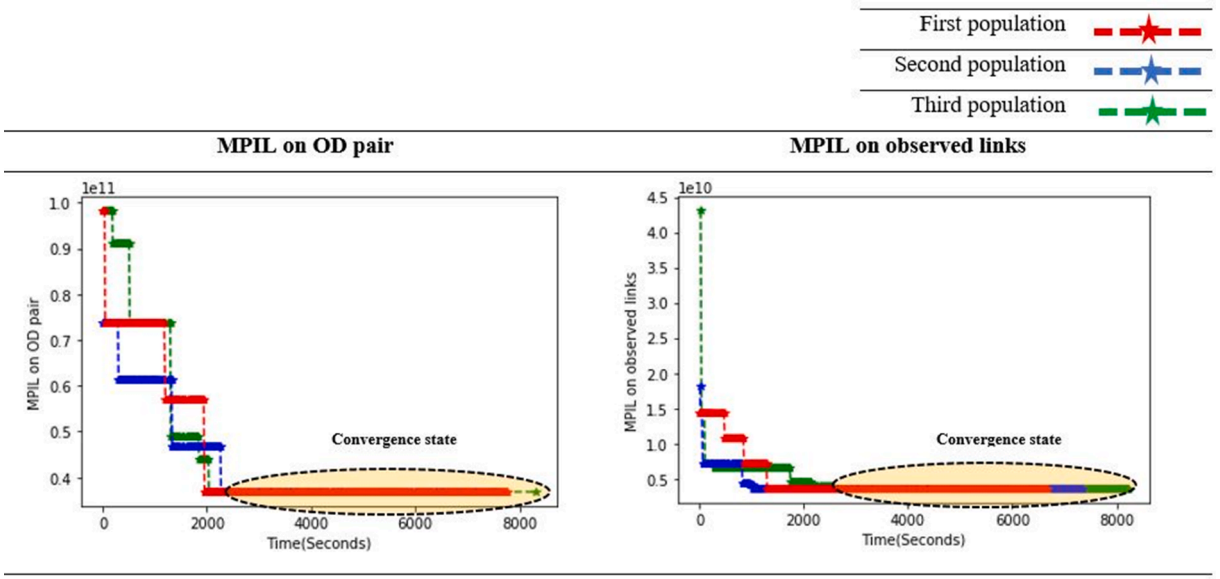

Fig. 16. Pattern of the GA for the Anaheim network.

includes all three possible failure scenarios in which one of the three sensors fail by time $s = 5$. This Figure also shows whether it is best to repair the failed sensors or to deploy new sensors in each scenario where similar to Table 9, the budget is set to 300 ($\times$ \$100).

The results of Fig. 13 indicate that the location of failed sensor can also affect the decision about the deployment of a new sensor or the repair of failed sensors. For instance, in the case of sensor failure on observed link 2, one new advanced sensor is installed on link 5, and one new basic sensor installed on link 15 without repairing the failed sensor on link 2 at the additional sensor deployment phase. On the other hand, where the sensor installed on link 16 fails, this sensor is decided to be repaired and the new advanced sensor is installed on link 18.

7.2.2. Additional sensor deployment concerning MPIL for OD pairs and observed links: Sioux Falls network

This section investigates the effect of the objective functions on the decision to repair failed sensors or to install new sensors in the Sioux Falls network. We borrowed the layout of existing sensors from the left side of Fig. 12 and assumed that these sensors were installed during the initial sensor deployment phase at time $s = 0$. We also assumed that when the additional sensor deployment phase occurs at time $s = 5$, the basic sensors installed on links 32, 55, and 62 will have broken down.

We used Eq. (16-I) as the objective function with different weights to determine which failed sensors should be repaired and to find new sensor locations. Scenario 1 in Fig. 14 weights the objective functions as $w_1 = 1 \& w_2 = 0$, which means this scenario focuses on minimizing the MPIL for OD pairs. Scenario 2 in the same Figure weights the objective functions to instead emphasize minimizing the MPIL for observed links. When we compare the choice between installing new sensors and repairing failed sensors, we can see that the objective functions have an impact on the outcome. The decision to install a new advanced sensor in a scenario is also impacted by the objective functions. For instance, the model decides to install a new advanced sensor on link 32 in scenario 1 because this link is connected to one of the OD pairs with the highest OD demand. In scenario 2, however, the new advanced sensor is installed on link 60, which is one of the links with the highest link flow.

7.3. Implementing the GA: Sioux Falls and Anaheim network

To implement the GA for each network at both the initial sensor deployment and additional sensor deployment phases, we generated three different population sizes and let the model run for a certain number of iterations for each population. This allowed us to observe the convergence rate patterns for the different populations. For each of the three populations, we explored the maximum number of iterations that needed to occur before a Convergence-state phase was achieved, where no better solution was obtained through subsequent iterations. We then multiplied this value by four to assure that there is not any fitness function improvement in the subsequent iterations.

For instance, the image on the left of Fig. 15 shows that the maximum number of iterations for the Sioux Falls was calculated to be 312, while the GA reached its maximum value before the 100th iteration for all three populations. Fig. 15 also shows the GA's convergence rate over time for the Sioux Falls network using different values of weights in Eq. (16-I). The left side of Fig. 15 shows the convergence of GA for the MPIL for OD pairs where $w_1 = 1$ and $w_2 = 0$. The right side of this figure, on the other hand, shows the

convergence of the GA for the MPIL for observed links where $w_1 = 0$ and $w_2 = 1$. The convergence-state phase with the lowest objective function value for all three populations (the weighted sum value) on both images in Fig. 15 is reached before time 1,120 ***s***[16] (around 19 min) and 1,050 ***s*** (around 17.5 min) for the left and right images, respectively. Note that the implementation of the GA also involved a degree of randomness, which resulted in different locally-optimized solutions for sensor locations in different populations instead of a globally optimized solution. Additional implementations may result in similarly locally-optimized solutions.

We also implemented the proposed GA for the Anaheim network, which is a relatively large network. To estimate OD demand for the Fishbone network and Sioux Falls network, we used the recently added nonlinear feature of Gurobi 9.1 to implement the ME formula introduced in Eqs. (27) and (28). For the Anaheim network, however, the nonlinear model implemented in Gurobi 9.1 significantly increased the total running time of the proposed GA. Therefore, we adopted another solution algorithm using the GA described in Appendix F to handle OD demand estimation. Note that the embedded GA for OD demand estimation does not necessarily provide the global optimal solution for OD demand values, but it was very effective at reducing the model's overall runtime.

The left side of Fig. 16 demonstrates the convergence of the GA for the MPIL on OD pairs where $w_1 = 1$ and $w_2 = 0$, and the right side shows the convergence of the GA for the MPIL on observed links where $w_1 = 0$ and $w_2 = 1$ in the Anaheim network. The maximum number of iterations for the Sioux Falls network in was calculated to be 1036 and 1118 for the left and right sides of Fig. 16, respectively. This number of iterations was achieved in 8300 ***s*** (2.3 h) and 8223 ***s*** (2.28 h) for the left and right sides of Fig. 16. The convergence-state phase with the lowest objective function value for all three populations (the weighted sum value) 15 is reached prior to 2273 ***s*** (around 37 min) and 2557 ***s*** (around 17.5 min) for the left and right sides of Fig. 16, respectively.

8. Conclusion

In this paper, we investigated the effect of time-dependent sensor failure on the NSLP for the OD estimation process for two distinct phases: the initial sensor deployment and at the additional sensor deployment. These two phases address the problem of sensor failure for sensor deployment at the planning phase, i.e., before the deployment of sensors in a road network, and during operation phases, i.e., with the presence of some already installed sensors in a road network. The introduction of the additional sensor phase addresses the need for routine/scheduled maintenance of existing sensors by instrumenting the network with additional sensors in new locations or repairing or replacing failed sensors. We introduced the novel concept of MPIL for OD demand flow during the OD estimation process for each OD pair and sensor-instrumented links. Consistent with the OD covering rule, sensor failure on observed links may not necessarily result in information loss pertaining to the OD demand flow. We addressed this aspect of the OD estimation problem by formulating a new mathematical model that can prioritizes the maximum OD demand information loss on links while identifying the optimal locations for traffic sensors.

We implemented the proposed models on Fishbone and Sioux Falls and Anaheim networks. For the initial sensor deployment phase, we showed how the time-dependent sensor failure rate can affect the MPIL through the sensors' lifetimes. We also studied the impact of the total number of sensors on the MPIL of OD pairs in the Fishbone network. The results indicate that as the number of similar sensors increases, there is a corresponding decrease in the aggregated MPIL for OD pairs. For the same total number of sensors, a sensitivity analysis demonstrated the positive effect of employing more advanced sensors (i.e., with lower failure rate), which reduced the MPIL for OD pairs. In comparison to basic sensors, advanced sensors appeared to have a greater positive effect on the aggregated MPIL for OD pairs. An analysis of the numerical results based on the model's output for the Sioux Falls network showed that the sensor location sets were dependent on the objective function that was used to determine the sensor deployment at the initial sensor deployment.

For the additional sensor deployment phase, we defined different possible scenarios of sensor failure among the sensors deployed in the Fishbone network during the initial sensor deployment phase. The results show that the decisions of whether to install a new sensor or to repair the failed sensor(s), as well as the locations of new sensors, depend on the location(s) of the failed sensor(s) and the budget constraint. The results for the Sioux Falls network demonstrate that the objective function can also affect this decision at the additional sensor deployment phase.

We used the Sioux Falls and Anaheim networks to examine the convergence rate of the proposed GA. Depending on the initial population size and the objective function, the GA for the Sioux Falls network reached a convergence state between 1,050 ***s*** and 1,120 ***s***. Instead of Gurobi using 9.1 for the Anaheim network, we used another GA for OD demand estimation to reduce the model's total runtime. For this network, the convergence state was reached in under 2,557 ***s*** using objective functions that minimized MPIL for observed links and OD pairs.

Other possible extensions of this research include applying the proposed model to the travel time estimation problem in a road network where sensor failure can impact the reliability of travel time estimation on links and routes (or paths). The proposed model can also be integrated with the link flow observability problem to identify the sensor location set that minimizes the adverse effects of sensor failure on both link flow inference and OD demand estimation.

CRediT authorship contribution statement

Mostafa Salari: Conceptualization, Methodology, Software, Formal analysis, Writing – original draft. **Lina Kattan:** Conceptualization, Methodology, Supervision, Resources, Funding acquisition, Writing – review & editing. **William H.K. Lam:**

[16] **Seconds**

Conceptualization, Supervision, Writing – review & editing. **Mohammad Ansari Esfeh:** Methodology, Visualization, Formal analysis. **Fu Hao:** Software, Visualization, Formal analysis.

Declaration of Competing Interest

The authors declare that they have no known competing financial interests or personal relationships that could have appeared to influence the work reported in this paper.

Acknowledgments

This work is financially supported by Natural Sciences and Engineering Research Council of Canada (NSERC) Discovery and Discovery Accelerator Supplement grants (RGPIN/03923-2014, RGPAS/00099-2020), Alberta Innovate Strategic Research Projects on Integrated Urban Mobility (G2018000894), and NSERC CREATE on Integrated Infrastructure for Sustainable Cities (CREATE/511060-2018). It is also jointly supported by a Postgraduate Studentship of the Hong Kong Polytechnic University, together with grants from the Research Grants Council of the Hong Kong Special Administrative Region, China (Project No. PolyU 152628/16E) and from the Dean's Reserve Committee of the Hong Kong Polytechnic University (Project No. ZVSA).

Appendix A

Assume that, given a subset of observed links, the true mean OD demand (q^*) and the estimated mean OD demand (q) must satisfy the following relationship:

$$\sum_{j\in J} t_{l,j} q_j - \sum_{j\in J} t_{l,j} q_j^* \;=\; 0 \;\forall l \in \widetilde{L} \tag{A-1}$$

where $t_{l,j}$ is the proportion of trips between the j^{th} OD pair using link l.

If $\lambda_j = \frac{q_j - q_j^*}{q_j}$ denotes the relative deviation between the estimated OD demand and the true OD demand, then we can update Eq. (A-1):

$$\sum_{j\in J} t_{l,j} q_j - \sum_{j\in J} t_{l,j} q_j^* \;=\; \sum_{j\in J} t_{l,j} q_j \left(\frac{q_j - q_j^*}{q_j}\right) \;=\; 0 \rightarrow \sum_{j\in J} t_{l,j} q_j \lambda_j = 0 \;\forall l \in \widetilde{L} \tag{A-2}$$

Considering $G(\lambda) = \sqrt{\frac{\sum_{j\in J} \lambda_j^2}{|J|}}$ as the measure of the average relative deviation in the estimated OD demand, the MPRE can be formulated as below:

$$MPRE(\lambda) = MaxG(\lambda) \tag{A-3}$$

$$\sum_{j\in J} t_{l,j} q_j \lambda_j = 0 \;\forall l \in \widetilde{L} \tag{A-4}$$

$$\lambda_j \geqslant -1 \;\forall j \in J \tag{A-5}$$

Using the toy example presented in Section 3, the MPRE for the first and the second sensor location sets can therefore be presented as follows (see Table A1):

Table A1
MPRE calculation for two sensor location sets.

1st set:$\{1,2\}$	2nd set:$\{3,4\}$
$maxG(\lambda) = max\sqrt{\frac{\lambda_1^2+\lambda_2^2+\lambda_3^2+\lambda_4^2}{4}}$	$maxG(\lambda) = max\sqrt{\frac{\lambda_1^2+\lambda_2^2+\lambda_3^2+\lambda_4^2}{4}}$
$7\lambda_1 + 7\lambda_2 = 0$	$7.5\lambda_1 + 7.5\lambda_3 = 0$
$3.5\lambda_3 + 3.5\lambda_4 = 0$	$7.5\lambda_1 + 3\lambda_2 + 7.5\lambda_3 + 3\lambda_4 = 0$
$\lambda_j \geqslant -1 \;\forall j \in J$	$\lambda_j \geqslant -1 \;\forall j \in J$
$maxG(\lambda) = 1$	$maxG(\lambda) = 1$

Appendix B

To introduce the normalization method, the following terms must be defined:

Payoff matrix: Assume that there are N objective functions and the optimal value of the i^{th}objective function is achieved for the value x_i^* of the decision variable vector. We must compute the value of the other $N-1$ objective functions for x_i^*. The vector $[f_1(x_i^*)..f_i(x_i^*)..f_N(x_i^*)]$constructs the i^{th} row of the payoff matrix where the values of the objective function are derived for x_i^*. Concerning all N objective functions, we can construct an$N \times N$ payoff matrix:

$$\Psi = \begin{bmatrix} f_1(x_1^*)..f_i(x_1^*)..f_N(x_1^*) \\ f_1(x_2^*)..f_i(x_2^*)..f_N(x_2^*) \\ . \\ . \\ . \\ f_1(x_N^*)..f_i(x_N^*)..f_N(x_N^*) \end{bmatrix} \tag{B-1}$$

Utopia point: The Utopia point is a point where all objective functions reach their optimal values simultaneously. If we represent the Utopia point as f^U, then the following vector shows the utopia points for the N objective functions:

$$f^U = [f_1(x_1^*)..f_i(x_i^*)..f_N(x_N^*)]$$

Nadir point and pseudo-nadir point: The nadir point is a point in the objective space denoted by f^N where all objective functions achieve their worst values. Assuming we initially aim to minimize N objective functions, then the following vector shows the nadir point for these functions:

$$f^N = \left[\max_{x\in\Omega} f_1(x)..\max_{x\in\Omega} f_i(x)..\max_{x\in\Omega} f_N(x)\right] \tag{B-2}$$

where $\Omega$is the feasible space. While calculating f^N, some elements of nadir points may become unbounded. Therefore, we use the Pseudo-nadir point denoted by f^{SN}, which is the Nadir point extracted from the payoff matrix. For example, we can find the pseudo-nadir point related to the i^{th} objective function using the following equation:

$$f_i^{SN} = max\{f_i(x_1^*), f_i(x_2^*), ...f_i(x_N^*)\} \tag{B-3}$$

The vector that presents the Pseudo-nadir point for the N objective functions is:

$$f^{SN} = [f_1^{SN}, f_2^{SN}, ..., f_N^{SN}] \tag{B-4}$$

Appendix C

We implemented the proposed GA using the Python programming language and Gurobi 9.1 on a personal computer with a 3.4 GHz Intel Core^{TM} i7-6700 processor and 16 GB of memory. In the context of this problem, a GA starts with an initialization procedure whose population size, chromosome representation approaches, and parameters are outlined in Table C1. During initialization, the algorithm constructs three different populations with distinctive sizes that are dependent on the size of the network. The primary reason for constructing different populations is to determine the appropriate number of iterations. The fitness function that determines the elite chromosomes corresponds with the objective functions that have been defined in Eqs. (16) and (17).

C.1. Chromosome representation

To represent a sensor's location in the GA, we define each chromosome length to be equal to the number of links in the road network. Each gene will be able to demonstrate whether a link is instrumented with a sensor. For instance, if the j^{th} gene of a chromosome is equal to 1, a sensor of type 1 should be installed on link j. If the same gene is equal to 0, link j should be unobserved. Chromosomes can represent feasible solutions for sensor location problems provided that they meet the OD covering rule. To generate feasible chromosomes in the initial sensor deployment phase, we use the following formulation, which employs the OD covering rule and the sensor assignment on observed links in the constraint set:

$$Z_{Chromosome} = min\left(\sum_{l\in L}\sum_{k\in K} c_l x_{k,l}\right) \tag{C-1}$$

s.t.,

Table C1
Settings related to the proposed GA.

Parameters	Description
Mutation rate	Discrete uniform distribution. Range: [0.2, 0.7]
Crossover rate	Discrete uniform distribution. Range: [0.4,0.9]
Initial population size	Three different population sizes. Population size varies depending on the size of a network.
Number of iterations (*MaxItr*)	4 × the maximum number of repetitions among different populations.

Eqs. (19) and (21)where c_l is the random cost assigned to link l. The optimal value of the decision variable represents the genes' values in a feasible chromosome. In other words, if $x_{k,l} = 1$, then l^{th} gene of the chromosome is equal to k. We need to update the chromosome generation mechanism in the additional sensor deployment phase. To generate feasible chromosomes in this phase, we use a function that is similar to Eq. (C-1) as the objective function, but where $x'_{k,l}$ is used as a decision variable in the objective function (Eq. (C-2)) and Eqs. (23) and (24) are used as constraints:

$$Z'_{Chromosome} = min\left(\sum_{l\in L}\sum_{k\in K} c_l x'_{k,l}\right) \tag{C-2}$$

s.t.,

Eqs. (23) and (24)

C.2. Crossover, mutation, and termination criteria

The crossover procedure increases the chance of reproduction of higher-ranked chromosomes concerning the fitness function. The mutation procedure supplements the crossover procedure by guaranteeing diversity in the subsequent population's generation. We must also determine the stopping criteria, also known as the termination condition, to identify the stopping point of the GA's generation process. Reaching a fixed number of repetitions, meeting the budget cap, and making no improvement in the fitness function through successive iterations are common terminating conditions. In this research, the proposed GA is terminated after a predetermined number of iterations. There is a possibility for an exhaustive number of iterations while we define the optimal number for the initial population. To avoid this, we implemented the GA with different initial populations. For each attempt, we defined the number of iterations as four times the maximum iterations among different populations in which there was no improvement in the successive iterations' fitness function.

Appendix D

Table D1 demonstrates the link flow on each link of the Fishbone network. The traffic flow on a link depends on the number of OD flows that traverse that link, which is converted to passenger car units (pcus) per hour.

To use the stochastic link choice proportion, we must define the initial link choice proportion between OD demands. In Table D2, the number of rows and columns represent the number of links and OD pairs in the Fishbone network, respectively. Each gene at the intersection of a row (representative of a link) and a column (representative of an OD pair) is a proportional representation of the flow

Table D1
Link flows (pcu/hr) in the Fishbone network.

Link ID	1	2	3	4	5	6	7	8	9
Link flow	585	125	325	465	320	105	195	225	460
Link ID	10	11	12	13	14	15	16	17	18
Link flow	405	420	215	270	240	850	650	620	880

of an OD pair that uses that specific link.

Table D2
Initial link choice proportion in the Fishbone network.

OD Link	1	2	3	4
1	0.49	0.54	0	0
2	0.51	0.46	0.65	0
3	0	0	0.35	0
4	0	0	0	1
5	0	0	0	0
6	0	0	0.65	0
7	0	0.46	0	0
8	0	0	0	1
9	0.49	1	0	0
10	0	0	0.65	0
11	0.51	0	0	0
12	0	0	0.35	1
13	0	0	0	0
14	0	0	0.35	0
15	1	1	0.35	0
16	0	0	0.65	1
17	1	0	1	0
18	0	1	0	1

Appendix E

The origin and destination nodes and the prior OD demands for the Sioux Falls network are presented in Table E1. According to this table, there are 30 OD pairs in the Sioux Falls network, where nodes 1, 6, 11, 13, 18, and 22 act as both origin and destination nodes for different OD pairs. The prior OD demand for the listed OD pairs ranges from 240 pcu/hr (OD3, OD19, OD24) to 840 pcu/hr (OD9, OD10, OD15, OD18, OD20, OD28). Note that the origin and destination nodes and the true OD demand values are adopted from Fu et al. (2019).

Table E1
OD demand information in Sioux Falls network.

OD#	OD nodes	True OD demands (pcu/hr)
1	1–6	480
2	1–11	600
3	1–13	240
4	1–18	600
5	1–22	600
6	6–1	360
7	6–11	600
8	6–13	600
9	6–18	840
10	6–22	840
11	11–1	360
12	11–6	480
13	11–13	480
14	11–18	720
15	11–22	840
16	13–1	360
17	13–6	600
18	13–11	840
19	13–18	240
20	13–22	840
21	18–1	480
22	18–6	480
23	18–11	600
24	18–13	240
25	18–22	840
26	22–1	480
27	22–6	360
28	22–11	840
29	22–13	720
30	22–18	480

Appendix F

In this appendix, we explain the GA developed to estimate OD demands based on ME method. The fitness function for OD demand estimation is according to Eq. (27). To represent the OD demand value in the GA, we define each chromosome length to be equal to the number of OD demands in a road network. Each gene will be able to exhibit the OD demand value of an OD pair. For instance, if the j^{th} gene of the chromosome is equal to q, this means that the j^{th} OD pair demand value is estimated to be q. Chromosomes can represent feasible solutions for OD demand estimation problems if they meet the traffic observation on observed links equipped with sensors. To generate feasible chromosomes in the initial OD demand estimation, we use the following formulation, which employs the traffic observation on observed links in the constraint set:

$$Z'_{Chromosome} = max\left(\sum_{j\in J} c_j q_j\right) \tag{F-1}$$

$$v_l = \sum_{j\in J} t_{l,j} q_j \ \forall l \in \widetilde{M} \tag{F-2}$$

where in Eq. (F-1), c_j is the random cost assigned to OD pair j. The optimal value of the decision variable, q_j represents the genes' values in a feasible chromosome. In other words, the optimal value of q_j from above optimization model will be represented in j^{th} gene of a chromosome. The above optimization model can be repeated until enough feasible chromosomes are generated. For crossover and mutation procedures, we employed a similar approach as discussed in Appendix C.

References

Aarset, M.V., 1987. How to identify a bathtub hazard rate. IEEE Trans. Reliab. R-36 (1), 106–108.

Bachir, D., Khodabandelou, G., Gauthier, V., El Yacoubi, M., Puchinger, J., 2019. Inferring dynamic origin-destination flows by transport mode using mobile phone data. Transp. Res. Part C: Emerg. Technol. 101, 254–275.

Balakrishna, R., Ben-Akiva, M., Koutsopoulos, H.N., 2019. Time-dependent origin-destination estimation without assignment matrices. Transport Simulation EPFL Press, pp. 201–213.

Bell, M.G.H., 1991. The estimation of origin-destination matrices by constrained generalised least squares. Transp. Res. Part B: Methodol. 25 (1), 13–22.

Bianco, L., Confessore, G., Reverberi, P., 2001. A network based model for traffic sensor location with implications on O/D matrix estimates. Transp. Sci. 35 (1), 50–60.

Bianco, L., Confessore, G., Gentili, M., 2006. Combinatorial aspects of the sensor location problem. Ann. Oper. Res. 144 (1), 201–234.

Bierlaire, M., 2002. The total demand scale: a new measure of quality for static and dynamic origin–destination trip tables. Transp. Res. Part B: Methodol. 36 (9), 837–850.

Cantelmo, G., Viti, F., Cipriani, E., Nigro, M., 2018. A utility-based dynamic demand estimation model that explicitly accounts for activity scheduling and duration. Transp. Res. Part A: Policy Pract. 114, 303–320.

Cantelmo, G., Viti, F., 2020. A Big Data Demand Estimation Model for Urban Congested Networks. Transp. Telecommun. J. 21 (4), 245–254.

Cao, Y., Tang, K., Sun, J., Ji, Y., 2021. Day-to-day dynamic origin–destination flow estimation using connected vehicle trajectories and automatic vehicle identification data. Transp. Res. Part C: Emerg. Technol. 129, 103241. https://doi.org/10.1016/j.trc.2021.103241.

Cascetta, E., Postorino, M.N., 2001. Fixed point approaches to the estimation of O/D matrices using traffic counts on congested networks. Transp. Sci. 35 (2), 134–147.

Cascetta, E., 2009. Transportation systems analysis: models and applications. Springer Science & Business Media.

Cascetta, E., Papola, A., Marzano, V., Simonelli, F., Vitiello, I., 2013. Quasi-dynamic estimation of o-d flows from traffic counts: Formulation, statistical validation and performance analysis on real data. Transp. Res. Part B: Methodol. 55, 171–187.

Castillo, E., Conejo, A.J., Menéndez, J.M., Jiménez, P., 2008. The observability problem in traffic network models. Comput.-Aided Civ. Infrastruct. Eng. 23 (3), 208–222.

Castillo, E., Nogal, M., Rivas, A., Sánchez-Cambronero, S., 2013. Observability of traffic networks. Optimal location of counting and scanning devices. Transportmetrica B: Transport. Dynamics 1 (1), 68–102.

Chen, A., Chootinan, P., Recker, W., Zhang, H. M., 2004. Development of a path flow estimator for deriving steady-state and time-dependent origin-destination trip tables.

Cerrone, C., Cerulli, R., Gentili, M., 2015. Vehicle-id sensor location for route flow recognition: Models and algorithms. Eur. J. Oper. Res. 247 (2), 618–629.

Chootinan, P., Chen, A., Yang, H., 2005. A bi-objective traffic counting location problem for origin-destination trip table estimation. Transportmetrica 1 (1), 65–80.

Danczyk, A., Di, X., Liu, H.X., 2016. A probabilistic optimization model for allocating freeway sensors. Transp. Res. Part C: Emerg. Technol. 67, 378–398.

de Dios Ortúzar, J., Willumsen, L.G., 2011. Modelling transport. John wiley & sons.

Doblas, J., Benitez, F.G., 2005. An approach to estimating and updating origin–destination matrices based upon traffic counts preserving the prior structure of a survey matrix. Transp. Res. Part B: Methodol. 39 (7), 565–591.

Ehlert, A., Bell, M.G.H., Grosso, S., 2006. The optimisation of traffic count locations in road networks. Transp. Res. Part B: Methodol. 40 (6), 460–479.

Eisenman, S.M., Fei, X., Zhou, X., Mahmassani, H.S., 2006. Number and location of sensors for real-time network traffic estimation and prediction: Sensitivity analysis. Transp. Res. Rec. 1964 (1), 253–259.

Florian, M., 2008. Models and software for urban and regional transportation planning: the contributions of the center for research on transportation. INFOR: Inform. Syst. Operat. Res. 46 (1), 29–49.

Fu, C., Zhu, N., Ling, S., Ma, S., Huang, Y., 2016. Heterogeneous sensor location model for path reconstruction. Transp. Res. Part B: Methodol. 91, 77–97.

Fu, H., Lam, W.H.K., Shao, H.u., Xu, X.P., Lo, H.P., Chen, B.Y., Sze, N.N., Sumalee, A., 2019. Optimization of traffic count locations for estimation of travel demands with covariance between origin-destination flows. Transp. Res. Part C: Emerg. Technol. 108, 49–73.

Fukushima, M., 1984. A modified Frank-Wolfe algorithm for solving the traffic assignment problem. Transp. Res. Part B: Methodol. 18 (2), 169–177.

Gan, L., Yang, H., Wong, S.C., 2005. Traffic counting location and error bound in origin-destination matrix estimation problems. J. Transp. Eng. 131 (7), 524–534.

Ge, Q., Fukuda, D., 2016. Updating origin–destination matrices with aggregated data of GPS traces. Transp. Res. Part C: Emerg. Technol. 69, 291–312.

Gentili, M., Mirchandani, P.B., 2005. Locating active sensors on traffic networks. Ann. Oper. Res. 136 (1), 229–257.

Gentili, M., Mirchandani, P.B., 2012. Locating sensors on traffic networks: Models, challenges and research opportunities. Transp. Res. Part C: Emerg. Technol. 24, 227–255.
Hadavi, M., Shafahi, Y., 2016. Vehicle identification sensor models for origin–destination estimation. Transp. Res. Part B: Methodol. 89, 82–106.
Hadavi, M., Shafahi, Y., 2019. Vehicle identification sensors location problem for large networks. J. Intell. Transp. Syst. 23 (4), 389–402.
Hazelton, M.L., 2000. Estimation of origin–destination matrices from link flows on uncongested networks. Transp. Res. Part B: Methodol. 34 (7), 549–566.
Hazelton, M.L., 2003. Some comments on origin–destination matrix estimation. Transp. Res. Part A: Policy Pract. 37 (10), 811–822.
Hu, S.-R., Peeta, S., Chu, C.-H., 2009. Identification of vehicle sensor locations for link-based network traffic applications. Transp. Res. Part B: Methodol. 43 (8-9), 873–894.
Hu, S.-R., Liou, H.-T., 2014. A generalized sensor location model for the estimation of network origin–destination matrices. Transp. Res. Part C: Emerg. Technol. 40, 93–110.
Oh, J.-S., Jayakrishnan, R., 2002. Emergence of private advanced traveler information system providers and their effect on traffic network performance. Transp. Res. Rec. 1783 (1), 167–177.
Kattan, L., Abdulhai, B., 2012. Sensitivity Analysis of an Evolutionary based Time Dependent Origin/Destination Estimation Framework. IEEE Trans. Intell. Transp. Syst. 13 (3), 1442–1453.
Kingman, J.F.C., 2005. Poisson processes. Encyclopedia of biostatistics 6.
Lo, H.P., Zhang, N., Lam, W.H.K., 1999. Decomposition algorithm for statistical estimation of OD matrix with random link choice proportions from traffic counts. Transp. Res. Part B: Methodol. 33 (5), 369–385.
Lu, L.u., Xu, Y., Antoniou, C., Ben-Akiva, M., 2015. An enhanced SPSA algorithm for the calibration of Dynamic Traffic Assignment models. Transp. Res. Part C: Emerg. Technol. 51, 149–166.
Meyer, M.D., Miller, E.J., 1984. Urban transportation planning: a decision-oriented approach.
Mínguez, R., Sánchez-Cambronero, S., Castillo, E., Jiménez, P., 2010. Optimal traffic plate scanning location for OD trip matrix and route estimation in road networks. Transp. Res. Part B: Methodol. 44 (2), 282–298.
Ng, ManWo, 2012. Synergistic sensor location for link flow inference without path enumeration: A node-based approach. Transp. Res. Part B: Methodol. 46 (6), 781–788.
Ng, ManWo, 2013. Partial link flow observability in the presence of initial sensors: Solution without path enumeration. Transp. Res. Part E: Logistics and Transportation Review 51, 62–66.
Nigro, M., Cipriani, E., del Giudice, A., 2018. Exploiting floating car data for time-dependent origin–destination matrices estimation. J. Intell. Transp. Syst. 22 (2), 159–174.
Osorio, C., 2019. Dynamic origin-destination matrix calibration for large-scale network simulators. Transp. Res. Part C: Emerg. Technol. 98, 186–206.
Owais, M., Moussa, G.S., Hussain, K.F., 2019. Sensor location model for O/D estimation: Multi-criteria meta-heuristics approach. Oper. Res. Perspect. 6, 100100. https://doi.org/10.1016/j.orp.2019.100100.
Qurashi, M., Ma, T., Chaniotakis, E., Antoniou, C., 2020. PC–SPSA: employing dimensionality reduction to limit SPSA search noise in DTA model calibration. IEEE Trans. Intell. Transp. Syst. 21 (4), 1635–1645.
Rubin, P., Gentili, M., 2021. An exact method for locating counting sensors in flow observability problems. Transp. Res. Part C: Emerg. Technol. 123, 102855. https://doi.org/10.1016/j.trc.2020.102855.
Salari, M., Kattan, L., Lam, W.H.K., Lo, H.P., Esfeh, M.A., 2019. Optimization of traffic sensor location for complete link flow observability in traffic network considering sensor failure. Transp. Res. Part B: Methodol. 121, 216–251.
Van Zuylen, H.J., Willumsen, L.G., 1980. The most likely trip matrix estimated from traffic counts. Transp. Res. Part B: Methodol. 14 (3), 281–293.
Viti, F., Rinaldi, M., Corman, F., Tampère, C.M.J., 2014. Assessing partial observability in network sensor location problems. Transp. Res. Part B: Methodol. 70, 65–89.
Xu, X., Lo, H.K., Chen, A., Castillo, E., 2016. Robust network sensor location for complete link flow observability under uncertainty. Transp. Res. Part B: Methodol. 88, 1–20.
Yang, H., Iida, Y., Sasaki, T., 1991. An analysis of the reliability of an origin-destination trip matrix estimated from traffic counts. Transp. Res. Part B: Methodol. 25 (5), 351–363.
Yang, H., Zhou, J., 1998. Optimal traffic counting locations for origin–destination matrix estimation. Transp. Res. Part B: Methodol. 32 (2), 109–126.
Yang, H., Yang, C., Gan, L., 2006. Models and algorithms for the screen line-based traffic-counting location problems. Comput. Oper. Res. 33 (3), 836–858.
Yen, J.Y., 1970. An algorithm for finding shortest routes from all source nodes to a given destination in general networks. Q. Appl. Math. 27 (4), 526–530.
Zhang, H., Seshadri, R., Prakash, A.A., Antoniou, C., Pereira, F.C., Ben-Akiva, M., 2021. Improving the accuracy and efficiency of online calibration for simulation-based Dynamic Traffic Assignment. Transp. Res. Part C: Emerg. Technol. 128, 103195. https://doi.org/10.1016/j.trc.2021.103195.
Zhou, X., List, G.F., 2010. An information-theoretic sensor location model for traffic origin-destination demand estimation applications. Transp. Sci. 44 (2), 254–273.
Zhu, N., Ma, S., Zheng, L., 2017. Travel time estimation-oriented freeway sensor placement problem considering sensor failure. J. Intell. Transp. Syst. 21 (1), 26–40.